Dear Editors,

In the ”file track changes” most, but not all changes are seen. It is not shown that five of the figures, Fig. 4, Fig. 6, Figs 9-11, have been altered. We hope that what we now submit is enough for you to accept publication. If not, please let us know as soon as possible.

Best regards

Svante Björck and co-authors

Interactive comment on “A south Atlantic island record uncovers shifts in westerlies and hydroclimate during the last glacial” by Svante Björck et al.

Anonymous Referee #1 Received and published: 4 July 2019

General comments: Björck et al. generated a multi-proxy record from a sediment core in a mid-latitude island of South Atlantic Ocean covering the last glacial (36.4- 18.6 ka) to reconstruct temperature and hydroclimate changes, both of which were linked with latitudinal movements of the southern hemisphere westerlies. PCA was used to reduce the dimensionality of multi proxy data. Isotope-enabled GCM was also included to investigate the controlling factors on precipitation d2H in the study area. The new South Atlantic record was compared with other paleoclimate records from northern hemisphere and other regions (both on continents and in oceans) to discuss the interhemispheric links during the last glacial. The manuscript was overall mature and well-written, but the section 5 of this manuscript is a bit hard to read, particularly for me to eyeballing Figs. 4, 6, 10, 11 at the same time. The contents and orders of these figures might be further improved.

Specific comments: L90 & L92: The setting of site is vague. It was a “overgrown crater lake” but also part of a “peat bog”?

L131 & L147: Could you explain what k-value is and how it is related to estimate sedimentation rate?

L264: if BIT is close to 1 steadily throughout the core, it does not mean any prerequisite for the valid use of brGDGTs-based proxies. BIT itself does not endorse anything considering its complexity in lake sediments. It only indicates low concentrations of crenarchaeol in the samples you analyzed. It could be that the paleo-lake is small and shallow without in-situ lake thaumarchaea community, or that the catchment soils are generally wet (Dirghangi et al., 2013).

L277-278: It is indeed possible and not surprising for lake sediments. This is why brGDGT data from adjacent catchment soils are needed to verify how much similarity in brGDGT compositions is between top sediments and adjacent soils, although the situation could be different during the last glacial and between different depositional environments (gyttja, peat, etc.). The brGDGT source is very important and could have shifts over long time scales. The TOC profile you presented suggested the lake sediments are “gyttja” over this period, but the input of soil organic matter seems still likely. If the percentage between lake OM and soil OM shifted over time, the organic geochemistry data might be tricky.

L300: Southern Annular Mode is a more popular term.

L304: Are you just using the raw proxy data as the input to run PCA? Have you standardized proxy data or logarithmized proxy data? Is it going to influence PCA results?

L386-390: It is very unclear to me. The influence of marine animals on organic matter d15N needs some reference citation. Is the signal from bird guano? Why marine bird signals are suggesting “more or less continuous of SHW”? Are winds driving upwelling and bring nutrients to harbor seabirds? Why rising d13C values are related with more “aquatic”

Kommentar [s1]: We understand that it may be difficult to eyeball those figures at the same time, but some also belong to the early result section and therefore come earlier. We realized very early that this may be a problem and have therefore tried our best to place the figs in an optimal and logical order. In addition, a few curves are shown more than once.

Kommentar [s2]: The long-term development of a not too deep lake is that it turns into a peat bog through over-growth, especially if there is time enough! We have changed the text.

Kommentar [s3]: The k-value is the parameter in the sediment deposition model which determines the number of deposition events per unit depth. In practice, this determines the variability of sedimentation rates and hence, the rigidity of the age-depth model. If k is set to a small value, the modelled sedimentation rates are allowed to be very variable, while bigger values will lead to more constant accumulation rates, and hence, a “more stiff” age-depth model. The k-parameter is well known to all OxCal users and extensively described and discussed in [Bronk Ramsey 2008, Quaternary Science Reviews, 27 (1-2), 42-60]. We added the reference in the text, so that the interested reader who is not aware of the concept can find more information on it.

Kommentar [s4]: Agreed. We therefore wrote ONE prerequisite, not THE prerequisite. It is not clear what the reviewer likes us to change here, but we changed to: 'A basic prerequisite for the use of...'

Kommentar [s5]: We agree with the reviewer. Given the 'cold bias' in the soil calibration for lakes (=warm bias for soils when using a lake calibration) it is possible that our record reflects changing sources. However, we do not find an obvious correlation between GDGT-derived temperature and two proxies for terrestrial influx, the C/N ratio and magnetic susceptibility. Lake calibration sets will already have a certain soil component in them, with some lakes in that set having more, others less soil-derived GDGTs. In any case, soil and lake-derived calibrations do move in the same general direction even though the slope and intercept are different. The most pragmatic approach is still to use a lake-based calibration set, and see to what extent it corroborates with other proxy evidence. Our reconstruction is in very good agreement with the Antarctic temperature reconstruction and also covaries with the other proxies used ... [1]

Kommentar [s6]: Changed.

Kommentar [s7]: We have used the raw data and variables were centered and standardized, as stated in chapter 3.13.

organic carbon (many freshwater plants can have negative d13C)? How can you infer “higher influence from C4 grasses” when you have already said “after which time aquatic sources become more important”? What’s the modern catchment vegetation composition?

L395: I agree with that n-alkane d2H data has good correspondence with diatom data. You may also have to think of the differential response between mid- and longchain alkane d2H. Both precipitation/source water d2H and evaporative enrichment can cause d2H shifts, but it is possible to separate these two signals by using the difference between terrestrial and aquatic plant biomarker d2H (Seki et al., 2011; Rach et al., 2014). Again, it is better to have some modern plant biomarker data at this site.

L414 & 428: You cannot use MST/MAT as a proxy for “winter temperature”. Pearson et al. (2011) gave a transfer function for summer air temperature for the reason that many of their lakes have strong seasonality: only summer is biologically important and only summer temperature is monitored. Most of intact brGDGT molecules were produced during summer. Again, winter has almost nothing to do with brGDGT-producing bacteria as the whole lake is frozen and catchment is covered by snow. Loomis et al. (2012) chose mean annual air temperature because most of their lakes are from highelevation tropics with very weak seasonality: every season is biologically important. Your study site is in subtropical mid-latitude and I expect your brGDGT data will be controlled by mean annual air temperature with a bit bias towards warmer/more productive summer, but you cannot just use that ratio to represent “winter temperature”. This is a misunderstanding on GDGT proxy itself.

L441, Fig. 7A: during the late Holocene simulation, the natural variability of d2H has a range of ~10 permil. Using correspondent maximum zonal wind latitude data, you can estimate the sensitivity of precipitation d2H to westerly core belt latitude, in unit of permil/degree latitude. This might be useful for paleo-westerly reconstruction. You may also note that the range of sediment core n-alkane d2H data are much larger than ~10 permil, indicating that (1) millennial-scale westerly latitudinal shifts have much larger amplitude than inter-annual scale of the late Holocene, and/or (2) sediment core d2H data, especially “aquatic” n-C23 have been dominated by variations in evaporative enrichment in lake water.

L432: The isotope GCM is simulating precipitation d2H variation, but not the lake water evaporation signal, although it is possible that drier conditions could cause increased raindrop re-evaporation below cloud, just like today’s Nevada and Arizona, but I am not sure if raindrop process is included in isotope GCM. The higher d2H values in model might indicate increasing contribution of low latitude moisture. If the westerly moved south, the island will be close to expanding subtropical zone, leading to increasing likelihood influenced by descending and warm (less negative d2H) air masses. If the westerly moved north, the island will be close to westerly core, receiving more moisture from polar air (more negative d2H), more similar to today’s 50 degree S condition.

L447: Is period of “1981-2010” within 20th century reanalysis? Should it be 1901- 2000? Is the gray lines in (B)-(D) are showing results from 20th century? Figure caption is incomplete.

L612: Why frost can be linked with weathering and CIA index?

Kommentar [s8]: We have now deleted some text and clarified some text and added a reference.

Kommentar [s9]: A modern plant dataset would be useful but only a full and complete study would give more insight than what is already known from other studies, and that falls outside the scope of this already very data-rich paper. On top, this is impossible to get anymore. Moreover this will reflect a modern plant community and not that of the LGM or before
Yes we have thought about the differential repsonse between terrestrial and aquatic dD. This can go various ways, as it depends a lot on the lake size, hydrology, climate, and terrestrial ecosystem. The approach in Rach et al and Seki et al is only valid when lakes are relatively insensitive to dryness and higher plants are more sensitive. However lake water (especially small shallow lakes like the one in this study) itself can also evaporate under dry summer conditions and thus change isotopically , whereas terrestrial lipids can be less sensitive because of a good groundwater reservoir that acts as a buffer. This situation turns the sensitivity towards drought around compared to the one used in Rach et al. - and is actually the sa ... [2]

Kommentar [s10]: We fully agree with the reviewer that this may not be a valid approach as a proxy for winter temperature. We have therefore deleted MST/MAT in the text, figures and PC ... [3]

Kommentar [11]: We think that a linear interpretation of the relationship between isotopic composition of precipitation and latitude is very risk ... [4]

Kommentar [12]: This is a very good comment and we have changed the text accordingly.

Kommentar [s13]: We have noted the importance of evaporative enrichment for n-C23 in the text already.

Kommentar [14]: This comment is assigned to wrong line number, possibly to lines below l. 453.

Kommentar [15]: Yes, this is included in the model, and now also in the text.

Kommentar [16]: This is what we mean on l. 461-465, but we have clarified it.

Kommentar [17]: We only use this period due to lack of SH data to constrain the reanalysis prior to the satellite era

Kommentar [18]: Yes, model in black and 20CR in gray. Figure caption is now completed.

Kommentar [s19]: The CIA index is linked to weathered material and mechanical weathering increases with temp changes causing periods below and above freezing.

L670: Is there any physical mechanism to explain the transition from unstable to stable climate mode? Technical corrections

L35: 4 k

L162: Xavg, avg subscript

L181: and 15N/14N

L193-194: bracket was missing

Kommentar [s20]: As we have noted slightly below it may be explained by the fact that we move from MIS3 to MIS2, and e.g. that the Subtropical Front (SF) moved north of Tristan, but the large scale processes behind this global scale change is still under debate.

Kommentar [s21]: Shouldn´t there be an ”a” to designate years? We think so.

Kommentar [s22]: Changed

Kommentar [s23]: Changed

Kommentar [s24]: Changed

Sid. 1: [1] Kommentar [s5] **seb** **2019-08-21 16:01:00**

We agree with the reviewer. Given the 'cold bias' in the soil calibration for lakes (=warm bias for soils when using a lake calibration) it is possible that our record reflects changing sources. However, we do not find an obvious correlation between GDGT-derived temperature and two proxies for terrestrial influx, the C/N ratio and magnetic susceptibility. Lake calibration sets will already have a certain soil component in them, with some lakes in that set having more, others less soil-derived GDGTs. In any case, soil and lake-derived calibrations do move in the same general direction even though the slope and intercept are different. The most pragmatic approach is still to use a lake-based calibration set, and see to what extent it corroborates with other proxy evidence. Our reconstruction is in very good agreement with the Antarctic temperature reconstruction and also covaries with the other proxies used in the PCA. In fact, when we now have removed the MAT and MAT/MST from the PCA we can compare the PC1 data with the MAT values and it shows a corr coeff of 75%! This is now included in the text. We therefore argue for a predominant influence of temperature, not source changes. To avoid confusion, we now only use the one from Loomis et al in the main text. We have adjusted the wording in our text reflecting the concerns of the reviewer, in line with the reply given here.

Sid. 2: [2] Kommentar [s9] **seb** **2019-08-21 16:04:00**

A modern plant dataset would be useful but only a full and complete study would give more insight than what is already known from other studies, and that falls outside the scope of this already very data-rich paper. On top, this is impossible to get anymore. Moreover this will reflect a modern plant community and not that of the LGM or before

Yes we have thought about the differential repsonse between terrestrial and aquatic dD. This can go various ways, as it depends a lot on the lake size, hydrology, climate, and terrestrial ecosystem. The approach in Rach et al and Seki et al is only valid when lakes are relatively insensitive to dryness and higher plants are more sensitive. However lake water (especially small shallow lakes like the one in this study) itself can also evaporate under dry summer conditions and thus change isotopically , whereas terrestrial lipids can be less sensitive because of a good groundwater reservoir that acts as a buffer. This situation turns the sensitivity towards drought around compared to the one used in Rach et al. - and is actually the same as the intepretation from the reviewer on the large dD variability of C23 (see below). We therefore refrain from using the approach by Rach and discuss the (covarying) terr and aquatic dD values separately and interpret the dD as mainly caused by circulation changes. The reviewer does not appear to be opposed by this so we leave our dD discussion as it is.

Sid. 2: [3] Kommentar [s10] **seb** **2019-08-21 16:10:00**

We fully agree with the reviewer that this may not be a valid approach as a proxy for winter temperature. We have therefore deleted MST/MAT in the text, figures and PCA. We have also deleted MAT in the PCA, as stated above.

Sid. 2: [4] Kommentar [11] **Unknown Author** **2019-08-20 10:22:00**

We think that a linear interpretation of the relationship between isotopic composition of precipitation and latitude is very risky due to the very dynamical processes in this region.

Clim. Past Discuss.,
https://doi.org/10.5194/cp-2019-65-RC2, 2019

Climate of the Past Discussions

Interactive comment on "A south Atlantic island record uncovers shifts in westerlies and hydroclimate during the last glacial" *by* Svante Björck et al.

Anonymous Referee #2

Received and published: 31 July 2019

This paper presents a comprehensive, multi-proxy analysis of a sediment core from South Atlantic Nightingale Island. The data are used to reconstruct past hydroclimate, temperature and Southern Hemisphere westerly winds. The authors then explore interhemispheric linkages, including evidence for DO events and the bipolar see saw connecting Greenland and Antarctic records, and relationships between past SHW strength and atmospheric CO2.

Abstract 23 The abstract is a series of rather unrelated statements. It needs to be rewritten following a standard structure, e.g.: 1. What problem did you study and why is it important? 2. What methods did you use to study the problem? 3. What were

Printer-friendly version

Discussion paper

your key findings? 4. What did you conclude based on these findings and what are the broader implications?

45 . . .(SHW) are a. . ..

48 . . .fluxes through physical. . .

75 This paragraph need to end with a clear statement of the aims of the paper – and how they will be addressed. Aims need to be presented in a logical order. For example using hydroclimate and temperature reconstructions to (1) reconstruct changes in the SHW in the Atlantic sector, (2) Identify interhemispheric linkages including evidence for DO events and the bipolar see saw linking Greenland and Antarctic records, and (3) determining if there is a link between past SHW strength and atmospheric CO2. Followed by a statement of why Nightingale Island is an ideal place to address these questions.

109 For each of the methods sections it would be helpful to state why the analysis was carried out in the leading sentence. E.g. on lines 285 and 291 there is no indication of why these analyses are being carried out.

133 Add something about the treatment of 14C outliers (in grey) on Figure 3. These are all younger ages so require an explanation. Lines 323-337 also avoids addressing this issue.

176 Provide a reference for this procedure.

328 Figure 4. It would be useful to have a common zoning system across all stratigraphic figures. The three PCA zones (line 489) dominate the discussion so I suggest using these here. It is not clear what the solid and dashed vertical black lines are on this figure – please explain in the caption. I strongly recommend plotting the 'productivity' indicators as fluxes (Cyperaceae pollen. Terrestrial diatoms, BSi, TOC) as this should provide a more accurate reconstruction of productivity through time.

399-347 These statements would be better placed in the methods. See comments on

Kommentar [s1]: The abstract is now totally altered.

Kommentar [s2]: Changed

Kommentar [s3]: Changed

Kommentar [s4]: We have now added this good suggestion into the text.

Kommentar [s5]: This has now been done for most of the methods.

Kommentar [s6]: We have now added explanations for the outliers.

Kommentar [s7]: This is something that is made routinely for C/N analyzes to account for differences in atomic weight: 14(N)/12(C) = 1.167. Added in the text.

Kommentar [s8]: This is done!

Kommentar [s9]: We find it unnecessary to explain that it shows every 500 and 1000 years.

Kommentar [s10]: We partly understand this point. For some of the proxies (e.g BioSi and TOC) it is impossible to calculate fluxes since we do not have dry density and since productivity is not the focus of the paper this can be done in a separate, more palaeo-ecologically focused paper, where we can present different types of pollen and diatom data. So we keep it as % for now, since we e.g. think that the relative impact of Cyperaceae may have influence on the alkanes.

Line 109 (above)

351 This statement needs qualifying. There are very few peak by peak similarities with EDML in these records – however I can see some reflection of the 3 PCA zones (line 489) across the different proxies.

357 State where these step changes are.

368 Figure 5. Please include a cluster analysis on this figure and also superimpose the PCA zones so that readers can see if the PCA zones are reflected in the pollen data. Ditto the diatom data (Fig. S2).

406 PCA – use capitals, cf. 417-418

555 and 622 Include the PCA zones on these figures as these are cited throughout the discussion.

581 State age and depth of this transition

586 Mark Antarctic LGM on figure

591 Replace 'good correspondence' with 'some correspondence'

604-609 The relationships with CO2 merit a separate subheading

630-653 This section could be strengthened by referring back to the original stated aims of the paper (see comments on Line 75 above).

676-678 This interpretation is not well-supported as the main phase of deglaciation was well after 18.6 Ka (see: Bentley, M. J., Ó Cofaigh, C., Anderson, J. B., Conway, H., Davies, B., Graham, A. C., Hillenbrand, C.-D., Hodgson, D. A., Larter, R. D., Mackintosh, A., and Verleyen, E.: A community-based geological reconstruction of Antarctic Ice Sheet deglaciation since the Last Glacial Maximum, Quaternary Science Reviews, 100, 1-9, 2014).

Kommentar [s11]: This is done and by a more detailed description of the methods and their utility.

Kommentar [s12]: Done! We have reformulated the similarities.

Kommentar [s13]: Done!

Kommentar [s14]: We refer once again to the point that the focus is not paleoecology, so for our purpose we only use selected pollen data for climate reconstructions. Therefore independent zonation of the pollen diagram (cluster analysis) is not relevant. Also, the pollen data does not indicate any major vegetation changes except for a few temp sensitive taxa. For the diatom data we concentrate on the ratios and not the percentages. So we think it is unnecessary, and the PCA zones are very clear in the diatom diagram without cluster analysis.

Kommentar [s15]: Done!

Kommentar [s16]: Done!

Kommentar [s17]: Done!

Kommentar [s18]: Antarctic LGM is not that well-defined! So we avoid it but discuss it in the text.

Kommentar [s19]: Done!

Kommentar [s20]: We disagree since this is only a small part of the discussion.

Kommentar [s21]: Good idea, but we moved it to the first part of the last section.

Kommentar [s22]: We have reformulated this so it is understood as the initial/start of the deglaciation.

A SOUTH ATLANTIC ISLAND RECORD UNCOVERS SHIFTS IN WESTERLIES AND HYDROCLIMATE DURING THE LAST GLACIAL

Svante Björck[1,2], Jesper Sjolte[1], Karl Ljung[1], Florian Adolphi[1,3], Roger Flower[4], Rienk H. Smittenberg[2], Malin E. Kylander[2], Thomas F. Stocker[3], Sofia Holmgren[1], Hui Jiang[5], Raimund Muscheler[1], Yamoah K. K. Afrifa[6], Jayne E. Rattray[7], Nathalie Van der Putten[8]

[1]Department of Geology, Lund University, SE-22362 Lund, Sweden
[2]Department of Geological Sciences and the Bolin Centre for Climate Research, Stockholm University, SE-10691 Stockholm, Sweden
[3]University of Bern, Physics Institute, Climate and Environmental Physics, Sidlerstrasse 5, CH-3012 Bern, Switzerland
[4]Department of Geography, University College London, London WC1E 6BT, UK
[5]Key Laboratory of Geographic Information Science, East China Normal University, 200062 Shanghai, PR China
[6]School of Geography, Earth and Environmental Sciences, University of Birmingham, Edgbaston, B15 2TT, UK
[7]Department of Biological Sciences, University of Calgary, Calgary, Canada
[8]Earth and Climate Cluster, Faculty of Science, Vrije Universiteit, Amsterdam, The Netherlands

Correspondence: Svante Björck (svante.bjorck@geol.lu.se)

Abstract

Changes in the latitudinal position and strength of the Southern Hemisphere Westerlies (SHW) are thought to be tightly coupled to important climate processes, such as cross-equatorial heat fluxes, Atlantic meridional overturning circulation (AMOC), the bipolar seesaw, Southern Ocean ventilation and atmospheric CO_2 levels. However, many uncertainties regarding magnitude, direction, and causes and effects of past SHW shifts still exist due to lack of suitable sites and scarcity of information on SHW dynamics, especially from the Last Glacial. Here we present a detailed hydroclimate multi-proxy record from a 36.4-18.6 ka old lake sediment sequence on Nightingale Island (NI). It is strategically located at 37°S in the central South Atlantic (SA) within the SHW belt and situated just north of the marine Subtropical Front (SF). This has enabled us to assess hydroclimate changes and their

link to the regional climate development as well as to large-scale climate events in polar ice cores. The NI record exhibits continuous impact of the SHW, recording shifts in both position and strength, and between 36-31 ka the westerlies show high latitudinal and strength-wise variability possibly linked to the bipolar seesaw. This was followed by 4 ka of slightly falling temperatures, decreasing humidity and fairly southerly westerlies. After 27 ka temperatures decreased 3-4°C, marking the largest hydroclimate change with drier conditions and a variable SHW position. We note that periods with more intense and southerly positioned SHW seem to be related to periods of increased CO_2 outgassing from the ocean, while changes in the cross-equatorial gradient during large northern temperature changes appear as the driving mechanism for the SHW shifts. Together with coeval shifts of the South Pacific westerlies, it shows that most of the Southern Hemisphere experienced simultaneous atmospheric circulation changes during the latter part of the last glacial. Finally we can conclude that multiproxy lake records from oceanic islands have the potential to record atmospheric variability coupled to large-scale climate shifts over vast oceanic areas.

~~The period 36-18 ka was a dynamic phase of the last glacial, with large climate shifts in both hemispheres. Through the bipolar seesaw, the Antarctic Isotope Maxima and Greenland DO events were part of a global "concert" of large scale climate changes. The interaction between atmospheric processes and Atlantic meridional overturning circulation (AMOC) is crucial for such shifts, controlling upwelling- and carbon cycle dynamics, and generating climate tipping points. Here we report the first temperature and humidity record for the glacial period from the central South Atlantic (SA). The presented data resolves ambiguities about atmospheric circulation shifts during bipolar climate events recorded in polar ice cores. A unique lake sediment sequence from Nightingale Island at 37°S in the SA, covering 36.4-18.6 ka, exhibits continuous impact of the Southern Hemisphere Westerlies (SHW), recording shifts in their position and strength. The SHW displayed high latitudinal and strength-wise variability 36-31~~

~~ka locked to the bipolar seesaw, followed by 4 ka of slightly falling temperatures, decreasing humidity and fairly southern westerlies. After 27.5 ka temperatures decreased 3–4°C, marking the largest hydroclimate change with drier conditions and a variable SHW position. We note that periods with more intense and southerly positioned SHW are correlated with periods of increased CO_2 outgassing from the ocean. Changes in the cross-equatorial gradient during large northern temperature changes appear as the driving mechanism for the SHW shifts. Together with coeval shifts of the South Pacific westerlies, it shows that most of the Southern Hemisphere experienced simultaneous atmospheric circulation changes during the latter part of the last glacial.~~

1 Introduction

The ~~Southern Hemisphere Westerlies (~~SHW~~)~~ are~~is~~ a major determinant of hydroclimate in the Southern Hemisphere (SH). In coupling marine and atmospheric processes, they are thought to have played a pivotal and multi-faceted role during and at the end of the last ice age by triggering changes in ocean-atmosphere CO_2 fluxes through~~by~~ physical processes (Saunders et al., 2018; Toggweiler and Lea, 2010) and Fe fertilization of the Southern Ocean through varying dust deposition (Lamy et al., 2014; Martin and Fitzwater, 1988; Martínez-García et al., 2014), as well as regulating the salt and heat leakage from the Agulhas current to the ~~Atlantic meridional overturning circulation (~~AMOC~~)~~ (Bard and Rickaby, 2009). In addition, changes in AMOC, SHW strength and position, and Southern Ocean upwelling seem to have been important mechanisms for different glacial CO_2 modes (Ahn and Brook, 2014). The position of the SHW during glacial times is debated with some arguing for a northward displacement (Toggweiler et al., 2006), while others argue for a southward move (Sime et al., 2013, 2016) during the Last Glacial Maximum (LGM), relative to the present. Holocene data also suggest an expanding-contracting SHW zone (Lamy et al., 2010). With these multiple scenarios the pattern of SHW shifts and their detailed role for ocean

Formaterat: Avstånd Före: 6,55 pt, Radavstånd: dubbelt

ventilation and the global carbon cycle remains unclear. It is postulated that the SHW moved in concert with rapid climate shifts recorded in Greenland ice cores known as Dansgaard-Oeschger (DO) cycles (Markle et al., 2016), and that these shifts are part of inter-hemispheric climate swings involving heat exchange between the hemispheres through the atmosphere and the ocean, with atmospheric heat fluxes partly compensating anomalous marine heat fluxes (Pedro et al., 2016). Whether SHW zonal shifts only occurred in the Pacific sector of the Southern Ocean (Chiang et al., 2014) or if they occurred throughout the SH is another crucial question (Ceppi et al., 2013). Other key climate issues relate to the effects and areal extent of the bipolar seesaw mechanism (Broecker, 1998; Stocker and Johnsen, 2003) and any signs of an early and long temperature minimum at southern mid-latitudes matching Antarctic LGM (EPICA Community Members et al., 2006). The lack of climate proxy records directly reflecting atmospheric conditions in the central South Atlantic means that such information at these latitudes during the glacial are primarily based on remote proxy records or climate model simulations. This results in a largely unconstrained understanding of glacial conditions over vast parts of the mid-South Atlantic, especially between 20-50°S where archives reflecting atmospheric processes are absent. In this study our aim is to use hydroclimate and temperature proxy records as well as climate model output to reconstruct changes in the position of the SHW in the Atlantic sector, reconstruct hydroclimate changes and identify interhemispheric linkages including the bipolar see-saw during the last glacial period. We also explore links between past SHW strength and atmospheric CO_2. For these questions the Tristan da Cunha archipelago is uniquely situated in the South Atlantic (Fig. 1A).

Formaterat: Teckensnitt:(Standard) Times New Roman, 12 pt

Formaterat: Teckensnitt:(Standard) Times New Roman, 12 pt

Formaterat: Teckensnitt:(Standard) Times New Roman, 12 pt

Formaterat: Teckensnitt:(Standard) Times New Roman, 12 pt

Formaterat: Teckensnitt:(Standard) Times New Roman, 12 pt

Formaterat: Teckensnitt:(Standard) Times New Roman, 12 pt

Formaterat: Teckensnitt:(Standard) Times New Roman, 12 pt

Formaterat: Teckensnitt:(Standard) Times New Roman, 12 pt

Formaterat: Teckensnitt:(Standard) Times New Roman, 12 pt

Formaterat: Teckensnitt:(Standard) Times New Roman, 12 pt

Formaterat: Teckensnitt:(Standard) Times New Roman, 12 pt, Nedsänkt

Formaterat: Teckensnitt:(Standard) Times New Roman, 12 pt

Formaterat: Teckensnitt:(Standard) Times New Roman, 12 pt

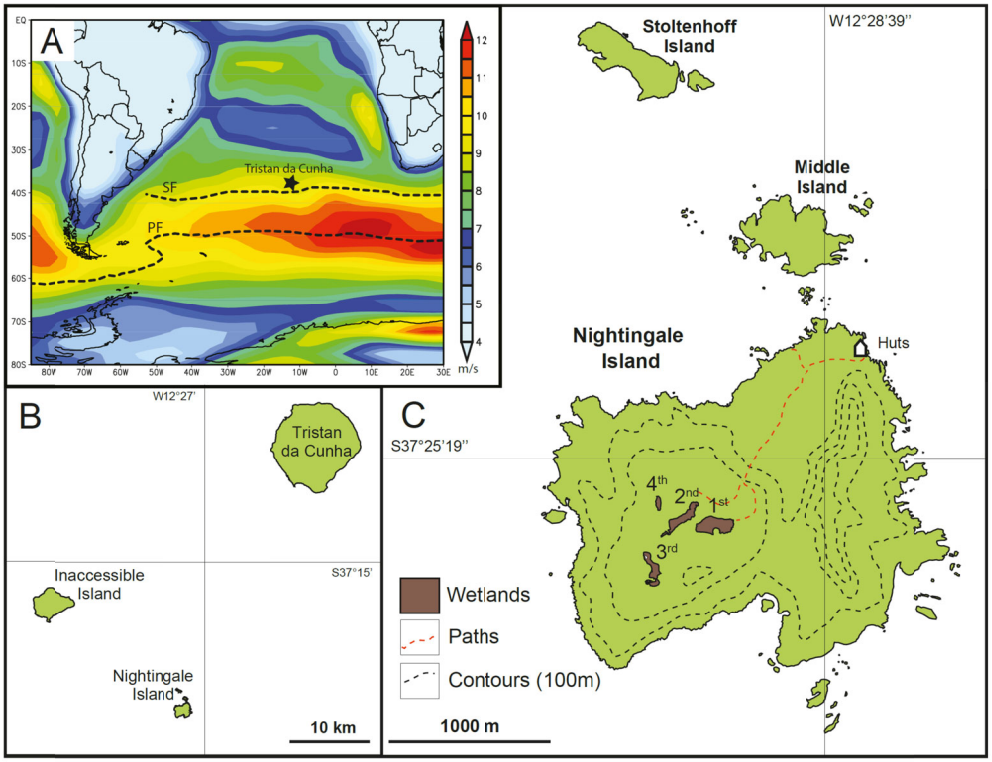

Figure 1. (A) The position of the Tristan da Cunha island group in the South Atlantic, the 1000mb mean annual wind speed (m/s) for 1980-2010 according to NCEP/NCAR reanalysis data indicating yellow-red colors for the zone of the Southern Hemisphere Westerlies, and the positions of the Subtropical Front (SF) and the Polar Front (PF) as dashed lines. (B) The three main islands of the Tristan da Cunha island group. (C) The position and size of the four overgrown lake basins, so-called ponds (1P-4P), on Nightingale Island with 100 m contour lines.

2 Study site

The Tristan da Cunha island group (TdC) at 37.1° S (Fig. 1) sits strategically at the northern boundary of the SHW (Fig. 1A), a few degrees north of the ~~Subtropical Front (~~SF~~)~~, where sea surface temperatures (SST) and salinities decrease by 3-4°C and 0.3 per mil, respectively. Annual mean air temperature and precipitation are 14.3°C and approximately 1500 mm, respectively, with highest precipitation in austral winter when the SHW impact is largest. The record presented here is from 1st Pond (1P), an overgrown crater lake (200x70 m, 207 m a.s.l.)

today forming a peat-bog in the central part of Nightingale Island (NI) (Fig. 1C and Fig. 2), a volcanic island dominated by trachytic bedrock. Its drainage area is about twice the size of ~~today's~~ the peat-bog and is thus sensitive to changes in the precipitation/evaporation balance (P/E). Previous studies from NI show that the area experienced shifts in precipitation during the Holocene (Ljung and Björck, 2007) and partly also during the Last Termination (Ljung et al., 2015), mainly attributed to the changing impact of the SHW. These data also indicate a southerly displacement of the Intertropical Convergence Zone (ITCZ) during the Heinrich 1 event (H1), and warming in the South Atlantic as a consequence of reduced AMOC, causing the lake basin to dry out, creating a hiatus between 18.6-16.2 ka (Ljung et al., 2015). Here we present a multi-proxy study of the sediments that accumulated before this hiatus dating to 36.4-18.6 ka, covering the younger part of Marine Isotope Stage 3 (MIS 3) and most of MIS 2, a climatically very dynamic period with Antarctic Isotope Maxima, DO and H events. In spite of its fairly northern position in relation to Antarctica we hypothesize that TdC was impacted by such events in terms of shifts of SHW, which we aim to test by using a suite of proxies.

Figure 2. Photograph from Nightingale Island. The over-grown lake basins of 1st and 2nd Pond are shown, with the higher situated 1st Pond in the background, seen towards southeast. Note the albatross chicks (white dots) and the four persons on 2nd Pond as scale. Photo S. Björck.

3 Material and methods

A large set of proxy data was analyzed, including chemical (N, XRF elemental concentrations and isotopes (^{13}C, ^{15}N, ^{2}H or D)), biological (TOC, molecular fossils such as *n*-alkanes, glycerol dialkyl glycerol tetraether lipids (GDGTs), pollen and diatom assemblages, biogenic silica (BSi)), and physical (magnetic susceptibility (MS)) parameters. Some proxies provide information about local changes such as soil conditions/erosion (C/N ratios, ^{13}C and MS),

weathering (major element data), vegetation composition (pollen, *n*-alkane distributions), organic productivity (TOC and BSi), lake conditions and levels (diatoms, BSi, δD values of short-chained *n*-alkanes) and bird impact (^{15}N). Others display regional changes in hydroclimate, such as mean annual air (MAAT) and mean summer air temperatures (MST) from the GDGT lipids and the source water of terrestrial and aquatic plants including evaporative conditions (hydrogen isotopes, δD). Observations of the isotopic content of precipitation are very sparse around TdC, and therefore we have investigated the hydroclimate variability with an isotope enabled climate model. In addition, we have performed principal component analysis (PCA) to distinguish the influence of the different proxies on samples (see Methods). Most of our data is found in the Supplementary data file.

3. 1 Field work, handling of cores and sample collection

Two weeks of field work on NI were carried out in February 2010 and drilling was carried out using Russian chamber samplers providing 1 m long cores (Ø=50 and 75 mm) with overlaps of 15-50 cm between each cored section. The ketch *Ocean Tramp* provided the transport from the Falkland Islands to TdC and back to Uruguay. In order to penetrate as deep as possible into the very stiff sediments a chain-hoist was used for coring the deeper parts of the sequences. The sediments were described immediately in the field before being wrapped in plastic film and PVC tubes. Upon arrival in Uruguay the cores were transported to the Geology Department in Lund where they were stored in a cold room. Before sub-sampling for the different proxy analyzes, the field-based lithostratigraphy and correlations between individual core sections were adjusted in the laboratory. This was aided by magnetic susceptibility (κ) measurements, which give a relative estimate of the magnetic mineral concentration, to confirm and adjust the visual correlation between overlapping core segments.

3.2 Radiocarbon dating and age model

The radiocarbon dated material consisted of 1 cm thick, organic-rich, bulk sediment. All 41 dated samples were pre-treated and measured at the Lund University Radiocarbon Dating Laboratory with Single Stage Accelerator Mass Spectrometry (SSAMS). The age model (Fig. 3) was constructed using the OxCal software package (Bronk Ramsey, 1995, 2009a). To minimize subjective user input we ran the age model with a general outlier model (Bronk Ramsey, 2009b), and a variable k-value that lets the model itself determine the sedimentation rate variability (Bronk Ramsey, 2008)~~Fig. 3)~~. For calibration we use the Southern Hemisphere calibration dataset, SHCal13 (Hogg et al., 2013)~~)~~.

3. 3 Measurements for magnetic susceptibility

Magnetic susceptibility (κ) was measured using a Bartington MS2E1 high resolution surface scanning sensor coupled to a TAMISCAN automatic logging conveyor. Measurements were carried out on non-sampled half cores and with a resolution of 5 mm and with results shown in 10^{-6} SI units. The magnetic susceptibility gives a relative estimate of the ability of the material to be magnetized, i.e. the magnetic mineral concentration.

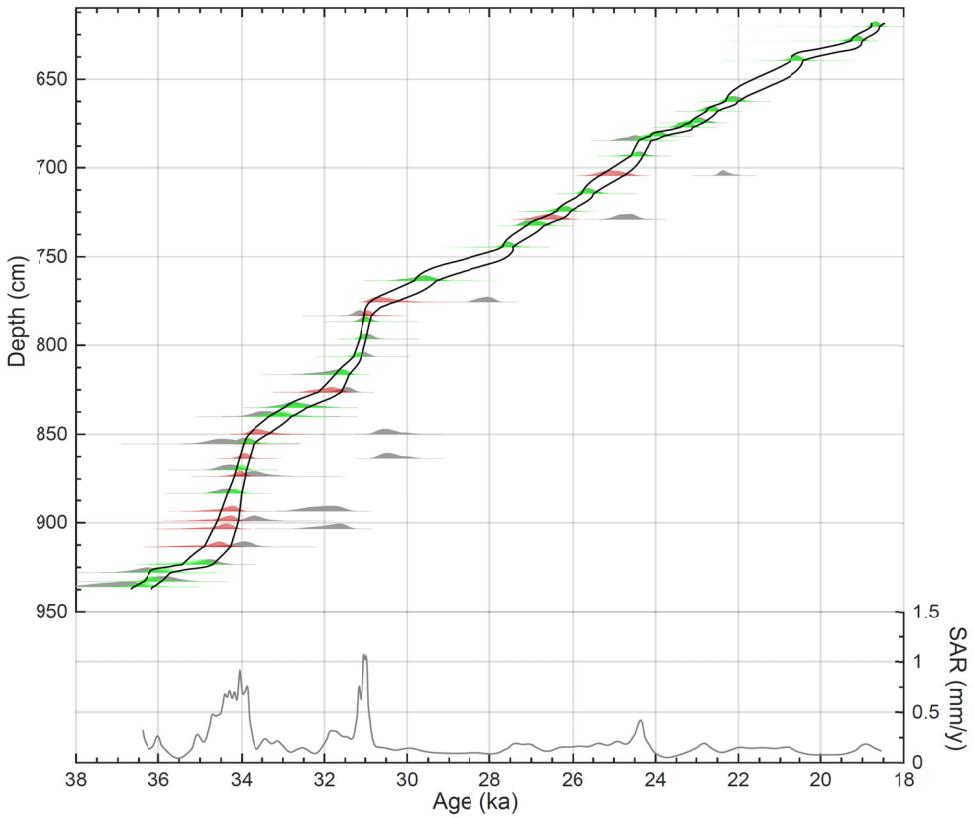

Figure 3. Age model for the sediments at 1st Pond, Nightingale Island. Top panel: Radiocarbon based age-depth model (black lines encompass the 68.2% probability interval). The patches indicate the calibrated probability distributions of each radiocarbon date for un-modelled (single) dates (grey patch), and their posterior distributions when modeled as a P-sequence: Green patches indicate agreement indices of >60% and red patches agreement indices of <60%, i.e., outliers. Bottom panel: Sediment accumulation rates (mm a^{-1}) based on the mean age-depth model shown in the top panel.

3. 4 XRF analyses

A handheld Thermo Scientific portable XRF analyzer (h-XRF) Niton XL3t 970 GOLDD+ set in the Cu/Zn mining calibration mode was used. The instrumentation provides highly accurate determinations for major elements (Helfert et al., 2011). All analyses were performed on freeze-dried sediments from the 1P cores using an 8 mm radius spot size in order to obtain representative values. The elemental detection depends partly on the duration of the analysis at each point; this is especially true for the lighter elements such as Mg, Al, Si, P, S, Cl, K and

Ca. For this reason the measurement time of each sample was set to 6 minutes. Although a larger suite of elements was acquired, we have chosen to work with Al, Si, P, S, K, Ca, Ti, Mn, Fe, Rb, Sr and Zr. These elements were selected based on their analytical quality (i.e., level above the detection limit) and with the help of Principal Component Analysis (PCA). PCA was made using JMP 10.0.0 software in correlation mode using a Varimax rotation. Before analysis all data were converted to Z-scores calculated as $(X_i-X_{avg})/X_{std}$, where X_i is the normalized elemental peak areas and X_{avg} and X_{std} are the series average and standard deviation, respectively, of the variable X_i. A Varimax rotation allocates into the components variables which are highly correlated (sharing a large proportion of their variance) – imposing some constrains in defining the eigenvectors. By grouping together elements showing similar variation, the chemical signals tend to be clearer and key elements are better identified. To simplify the interpretation of our principal components (PC) we employ a modified Chemical Index of Alteration (CIA), see Fig. 4D, as defined by Nesbitt and Young (1982): CIA = $[Al_2O_3/(Al_2O_3 + CaO + NaO + K_2O)] \times 100$. This index expresses the relative proportion of Al_2O_3 to the more labile oxides and is an expression of the degradation of feldspars to clay minerals. Since we have no NaO data we call it a *modified* CIA.

Formaterat: Nedsänkt

3.5 C and N analyses

Dried and homogenized samples every 1-2 cm were analysed with a Costech Instruments ECS 4010 elemental analyzer. The accuracy of the measurements is better than ± 5% of the reported values based on replicated standard samples. To account for C/N atomic ratios the ratio was ~~were obtained by~~ multipl~~y~~ied~~ng~~ by 1.167.

3.6 ^{13}C and ^{15}N analyses

Dried homogenized bulk samples were measured using a ThermoFisher DeltaV ion ratio mass spectrometer. The isotopic composition of samples is reported as conventional δ-values in parts per thousand relative to the Vienna Pee Dee Belemnite (^{13}C) and atmospheric ^{14}N (^{15}N):

Formaterat: Upphöjd

228 δ_{sample} (‰) = [(R_{sample}-$R_{standard}$)/($R_{standard}$)] x 1000 where R is the abundance ratio of $^{13}C/^{12}C$ in
229 the sample or in the standard.

230 ## 3.7 Pollen analyses

231 Sixty-four levels were sub-sampled and analysed for their pollen content. Pollen samples of 1
232 cm^3 were processed following standard method A as described by Berglund and Ralska-
233 Jasiewiczowa (1986) with added *Lycopodium* spores for determination of pollen concentration
234 values. Counting was made under a light microscope at magnifications of x400 and x1000.
235 The aim was to count at least 500 pollen grains in every sample, which was almost achieved
236 (mean sum of 565 pollen grains and mean sum of 870 pollen grains and spores). Identification
237 of pollen grains and spores was facilitated by published photos (Hafsten, 1960), standard
238 pollen keys (Moore et al., 1991) and a small collection of type slides from Tristan da Cunha
239 borrowed from The National History Museum in Bergen. The pollen percentage diagram (Fig.
240 5) was plotted in C2 (Juggins, 2007). Warm/cold pollen ratios were calculated as ($W_p/W_p + C_p$), where warm pollen types (W_p) are from plants only found below 500 m a.s.l. and cold
241
242 pollen types (C_p) are from plants only found above 500 m a.s.l.

243 ## 3.8 Diatom analyses and diatom environmental ratios

244 179 levels of 0.5 cm thick sediment segments were sub-sampled to analyse their diatom
245 content. For preparation of diatom slides ~ 200 mg freeze-dried sediment was oxidized with
246 15% H_2O_2 for 24 hours, then 30% H_2O_2 for a minimum of 24 hours, and finally heated at
247 90°C for several hours. A known quantity of DVB (divinylbenzene) microspheres was added
248 to 200 µL aliquots of the digested and cleaned slurries in order to estimate diatom
249 concentrations (Battarbee and Keen, 1982). The diatoms were mounted in Naphrax® medium
250 (refractive index = 1.65). 300 valves or more per sample were counted in most samples and
251 identified largely using published diatom floras (Krammer and Lange-Bertalot, 1986; Lange-
252 Bertalot, 1995; Le Cohu and Maillard, 1983; Moser et al., 1995; Van de Vijver et al., 2002).

253 Diatom results are expressed as relative % abundance of each taxon (Fig. S3) and also as total
254 concentrations of valves per g dry sediment.
255 Freshwater diatom species are excellent indicators of water quality, particularly
256 of pH, conductivity and dissolved nutrients (Battarbee et al., 2001). Sedimentary diatom
257 assemblages *inter alia* can be used to reconstruct past changes in water quality using the
258 ecological indicator information for each species. Where suitable modern diatom–water
259 quality calibration data sets exist transfer functions can be generated to reconstruct these
260 changes. However, in sediment records where diatom diversity is low and affinities of some
261 species are not firmly established, placing diatom taxa into ecological/environmental
262 preference groups using literature attributions and field experience can be used to generate
263 ratio scores relevant to past conditions. The 1st Pond assemblages are suitable for such an
264 approach, particularly for inferring changes in habitat and water acidity. The acid diatom
265 index ratio is derived from the sum of acid water indicating taxa comprising *Aulacoseira*,
266 *Frustulia*, *Pinnularia* and *Eunotia* compared to that of the fragilarioid tychoplanktonic taxa.
267 Proportions of acidity tolerant to acidity intolerant diatom taxa indicate water pH, total
268 tychoplankton (temporary phytoplankton) vs. total benthic taxa relate to open water
269 conditions, subaerial/terrestrial taxa vs. the total assemblage indicate wetland development
270 and/or in-washed material.

271 **3.9 Biogenic silica analyses**

272 The 310 samples were analyzed using a wet-alkaline digestion technique (Conley and
273 Schelske, 2001). Samples were freeze-dried and gently ground prior to analysis.
274 Approximately 30 mg of sample was digested in 40 ml of a weak base (0.47M Na_2CO_3) at
275 85°C for a total duration of 3 hours. Subsamples of 1 ml were removed after 3 hours and
276 neutralized with 9 ml of 0.021 M HCl. Dissolved Si concentrations were measured with a
277 continuous flow analyzer applying the automated Molybdate Blue Method (Grasshoff et al.,

1983). Biogenic silica content in lake sediments is a rough proxy for lake productivity.

3.10 Lipid biomarker and compound specific hydrogen isotopic analyses

The hydrogen isotopic composition (δ notation) of *n*-alkanes was analyzed by gas chromatography–isotope ratio monitoring–mass spectrometry (GC-IRMS) using a Thermo Finnigan Delta V mass spectrometer interfaced with a Thermo Trace GC 2000 using a GC Isolink II and Conflo IV system. Helium was used as a carrier gas at constant flow mode and the compounds separated on a Zebron ZB-5HT Inferno GC column (30 m x 0.25 mm x 0.25µm). Lipid extraction was performed on freeze-dried samples by sonication with a mixture of dichloromethane and methanol (DCM-MeOH 9:1 v/v) for 20 minutes and subsequent centrifugation. The process was repeated three times and supernatants were combined. Aliphatic hydrocarbon fractions were isolated from the total lipid extract using silica gel columns (5% deactivated) that were first eluted with pure hexane (F1) and subsequently with a mixture of DCM-MeOH (1:1 v/v) to obtain a polar fraction (F2). A saturated hydrocarbon fraction was obtained by eluting the F1 fraction through 10% $AgNO_3$-SiO_2 silica gel using pure hexane as eluent. The saturated hydrocarbon fractions were analyzed by gas chromatography – mass spectrometry for identification and quantification, using a Shimadzu GCMS-QP2010 Ultra. C_{21} to C_{33} *n*-alkanes were identified based on mass spectra from the literature and retention times. The concentrations of individual compounds were determined using a calibration curve made using mixtures of C21-C40 alkanes of known concentration. More details about the GC-IRMS method, including GC oven temperature program, instrument performance and reference gases used, are given in Yamoah et al. (2016). The average standard deviation for δD values was 5‰. Due to low sea levels during the time period of our proxies the δD values of the *n*-alkanes were ice volume corrected (Tierney and deMenocal, 2013), $\delta D_{corr} = (\delta D_{wax}+1000)/(\delta O^{18}_{w}*8*0.001+1)-1000$, with interpolated ocean water δO^{18}_{w} values (Waelbroeck et al., 2002).

Isoprenoid and branched glycerol dialkal glycerol tetraethers (GDGTs) were measured on the F2 fractions after filtration through 0.45 µm PTFE filters and reconstitution into a known volume of methanol. Analysis was done using a Thermo-Dionex HPLC connected to a Thermo Scientific TSQ quantum access triple quadrupole mass spectrometer, using an APCI interface. Chromatographic separation was achieved using a reverse phase method similar to the one used by Zhu et al. (2013). Partially co-eluting GDGT isomers were integrated as one peak in order to obtain data comparable to the normal phase method that has been in use by the community since Weijers et al. (2007).

A basic~~One~~ prerequisite for the valid use of brGDGTs is a relatively high branched-over-isoprenoid tetraether (BIT) index, which was 1.00 throughout the core. Reconstructed pH values, based on the CBT ratio (Weijers et al., 2007) were stable at 6.6 ±0.1 over the length of the core, which means that temperature is the dominant environmental factor exerted on the brGDGT distribution. At the time of measurement, we had not adopted the new method which separates between 5-methyl and 6-methyl branched GDGTs (De Jonge et al., 2014). As a consequence, we do not have individual quantifications of 5-methyl and 6-methyl branched GDGT isomers needed to use the revised MBT_{5me} temperature proxy for mineral soils (De Jonge et al., 2014) or peat (Naafs et al., 2017), which gives lower RMSE than the original terrestrial (soil) calibration (Weijers et al., 2007). However, since our data are from lake sediments, we argue that GDGT-based temperature proxy calibrations based on lake surveys is in any case a more valid approach. Indeed, using the original temperature calibration of Weijers et al. (2007) based on soils, resulted in very low temperatures between 0 and 6°C, a cold bias observed in other studies from lakes. This bias is probably due to the addition of *in situ* produced brGDGTs on top of any brGDGTs eroded from land (Loomis et al., 2012; Pearson et al., 2011). Our record could be biased by a changing ratio of soil- and lake-derived GDGTs, where a greater relative contribution of terrestrial-derived GDGTs

would result in a warm bias, if a lake calibration is used. However, we do not find a correlation between GDGT-derived temperature and two proxies for terrestrial influx, the C/N ratio and magnetic susceptibility, but rather the opposite. We ~~therefore~~ used ~~the~~two lake ~~global~~ calibration sets: a) the one of Pearson et al. (2011), based on a global lacustrine data set and using mean summer temperatures (MST), including samples from nearby South Georgia Island in the S. Atlantic, and b) ~~. In addition, we also use~~ a calibration based on a large data set of East African lakes from different altitudes (Loomis et al., 2012), using mean annual temperatures (MAAT), and which is also applicable outside of East Africa (Loomis et al., 2012). It is impossible to test which of these two proxy records would reflect past conditions more accurately. However, the two reconstructions strongly co-vary, with a difference between reconstructed MST and MAAT of approximately 5°C.

3.11 Calculation of insolation values

A long term numerical solution for Earth´s insolation quantities (Laskar et al., 2004) was used for the insolation values, 37-18 ka at 37°S, and calculated with the Analyseries program. While the austral winter values (W/m2) were based on mean daily June-August insolation (W/m2), the mean austral summer values were based on the mean daily December-February insolation.

3.12 Isotope model simulation

The isotope model analysis is based on a 1200-year simulation using the isotope enabled version of the ECHAM5/MPIOM earth system model (Werner et al., 2016) run with natural and anthropogenic forcings for 800 to 2000 CE (Sjolte et al., 2018). Horizontal resolution of the atmosphere is 3.75^{o} x 3.75^{o} (T31) with 19 vertical layers, while the ocean has a horizontal resolution of 3^{o} x 1.8^{o} with 40 vertical layers. The model includes isotope fractionation for all phase changes in the hydrological cycle, including below cloud evaporation. Since both the present day situation and our Nightingale Island record show a continuous impact from the

westerlies we deem it valid to use this late Holocene simulation as an analogue for interpreting the variability of the westerlies during the time period of study. The outcome of the simulation is presented in the result section, but further investigation of the model run shows that the multi-decadal variability of δD at TdC is related to the phase of the Southern ~~Antarctic~~ Annular Mode, indicating that isotopic variability at TdC is sensitive to large scale SH climate variability (Fig. S4).

3.13 Principal component analysis (PCA)

PCA was performed with 14~~-16~~ of our ~~variables (~~proxies (Fig. 6B) that we expect to respond to hydroclimate changes, but without the MAAT values in order to test the MAAT values vs. other climate proxies, using the C2 program (Juggins, 2007). The aim was to display the impact of different combination of proxies on the samples in a biplot (Fig. 6B), as discussed in Section 4.2. ~~Our two temperature proxies MAT and the MST/MAT ratio were both included and excluded in the analyses and this resulted in almost identical bi-plots in terms of positions of the variables. When the temperature proxies are excluded PC1 is slightly weaker (38.1 vs 40.9%) while PC2 is slightly stronger (13.4 vs 11.8%) than when they are included. We therefore include the temperature proxies in our PCA to illustrate temperature together with the other proxies.~~ All proxy data~~the variables~~ was~~ere~~ centered and standardized before calculation.

4. Results

4. 1 An island record of glacial climate in central South Atlantic

Thirty-nine 1 m long overlapping cores were taken in February 2010 from three over-grown crater lakes (Fig. 1C) between lava ridges (Anker Björk et al., 2011). 1P was exceptional in that it was the only site where sediments older than 18.6 ka were recovered. At 1P the 16.2-

377 18.6 ka hiatus (Ljung et al., 2015) is marked by a thin silt lamina at 618.8 cm. We retrieved
378 five overlapping cores below the hiatus with 318.2 cm of sediments before coring was
379 obstructed at 937 cm by suspected bedrock or boulders. These cores were correlated by
380 lithology and magnetic susceptibility (MS). The lower 162 cm consist of a dark brown
381 slightly silty gyttja, overlain by a grey brown silty clay gyttja, all deposited under anaerobic
382 conditions. Because of the low concentration of plant macro-fossil remains our chronology is
383 based on 41 ^{14}C dates of 1 cm thick bulk sediment samples between 620 and 936 cm (Table
384 S1). Comparisons of ^{14}C dates of bulk sediment and plant remains (wood and peat) have
385

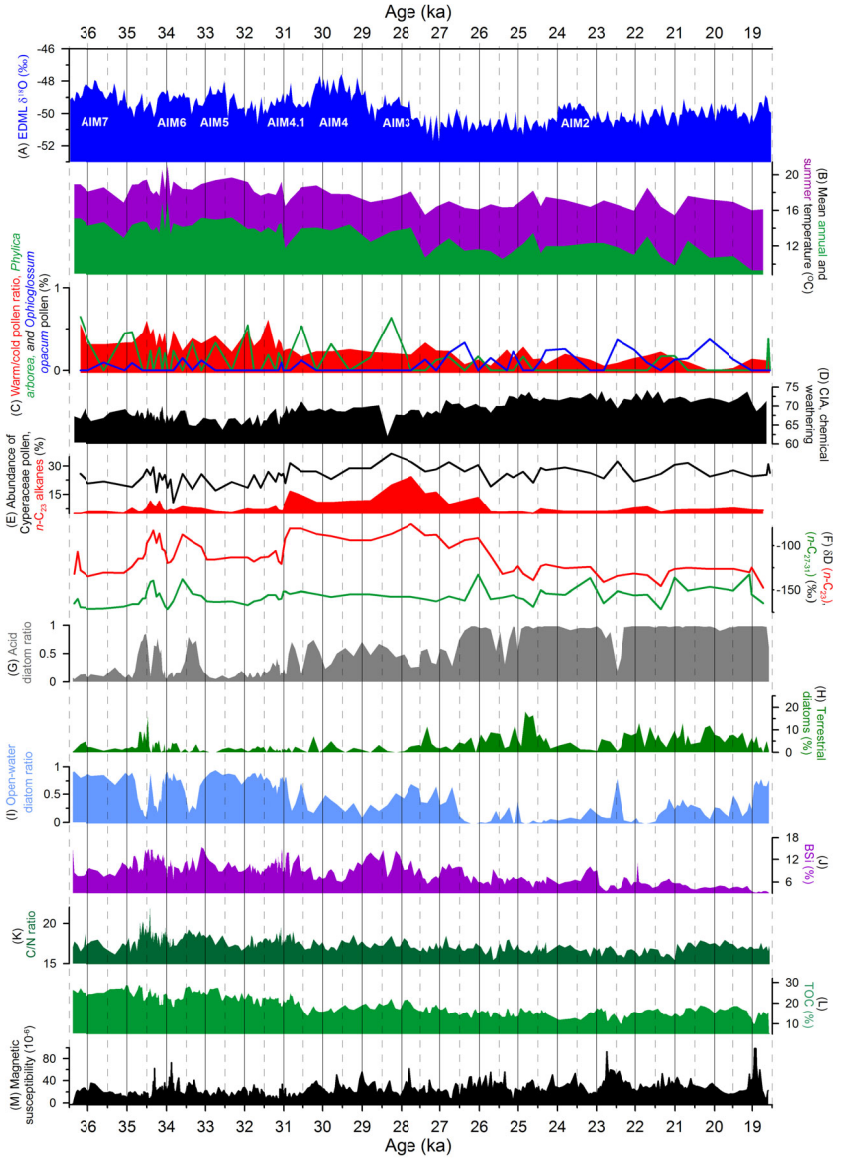

Figure 4. Antarctic ice core data and some of the proxy data from the sediments in 1st Pond, between 36.4 and 18.6 ka. (A) The EDML $\delta^{18}O$ record (EPICA Community Members, 2006) showing AIM 7-2. (B) GDGT-based ~~M~~mean annual air (MAAT) and summer temperature (MST)~~from the GDGT analyses and~~ calibrated to~~with~~ Pearson et al. (2011) and Loomis et al. (2012), respectively. (C) Warm pollen ratios, % *P. arborea* pollen and % *Ophioglossum* spores. (D) Modified chemical index of alteration (CIA). (E) % Cyperaceae pollen and *n*-C_{23} alkanes. (F) δD values (‰) of *n*-C_{23} and *n*-$C_{27\text{-}31}$ alkanes. (G) Acid diatom ratios. (H) % terrestrial diatoms. (I) Open water diatom ratios. (J) % biogenic silica (BSi). (K). C/N ratios. (L) % total organic carbon (TOC). (M) Magnetic susceptibility (MS) expressed as 10^{-6} SI units. All proxies are related to the age scale on the x-axes. Note that the two thick gray lines (31 ka and 26.5 ka) indicate the position of the three PCA zones (Fig. 6).

shown good concordance (Ljung et al., 2015; Ljung and Björck, 2007), and the most likely explanation for the seven clear outliers is possibly a combination of statistical noise and contamination of recent material. Our age model (Fig. 3) displays a mean sedimentation rate of 0.18 mm yr^{-1}, but with considerable variation.

~~A large set of proxy data from 1P (Figs. 4-5, Figs. S1-S3, Table S2) was analyzed and provides information about local changes such as soil conditions/erosion, weathering, vegetation composition, organic productivity, lake conditions and P/E ratios. Other proxies (GDGTs) display regional changes in temperature such as mean annual (MAT) and mean summer temperatures (MST) and hydroclimate conditions (deuterium isotopes), such as the source water of terrestrial and aquatic plants including evaporative conditions. Principal component analysis (PCA) was performed to investigate co-variability between proxies, showing the interplay of changes in hydroclimate driven by oceanic and atmospheric circulation changes (Fig. 6).~~

In agreement with the supposed minimum age of pond formation through volcanic activity (Anker Björk et al., 2011), the bottom of 1P has an age of 36.4±0.3 ka. Our temperature records (Fig. 4B) show an oscillating pattern, with the largest change at 27.5 ka, and share ~~many~~ similarities with the low frequency variability of the EDML curve (Fig. 4A). Before 27.5 ka MAT and MST vary between 17-12°C and 21-17°C, respectively, while the variation is between 13-9°C and 18.5-15.5°C, respectively, after 27.5 ka. In terms of pollen as a local temperature indicator it is known that *Phylica arborea*, *Acaena sarmentosa* and two Asteracea plant types are sensitive to cold conditions (Ryan, 2007). They make up warm pollen types at NI and the warm/cold pollen-types ratio (Fig. 4C) shows large variations until 31.4 ka, followed by a two-step decline (at 31.2 and 26.5 ka) largely in contrast to the spore abundance of the cold tolerant *Ophioglossum opacum* fern, and with a trend similar to the temperature curves. In comparison to Holocene sediments from NI (Ljung and Björck, 2007),

428 the glacial pollen record from 1P (Fig. 5) shows less variability, and the most distinct
429 difference is the very low abundance of the only tree species pollen on the island, the frost
420 limited *P. arborea*. Based on lapse rates, with 65-130 m lower sea levels 35-18 ka (Lambeck
421 et al., 2014), and today´s distribution of *P. arborea* on TdC and Gough Island (Ryan, 2007) we
422 can estimate that its absence after 28 ka implies minimum winter temperatures at least 3°C
423 lower than today, which agrees well with our MAAT curve (Fig. 3B).

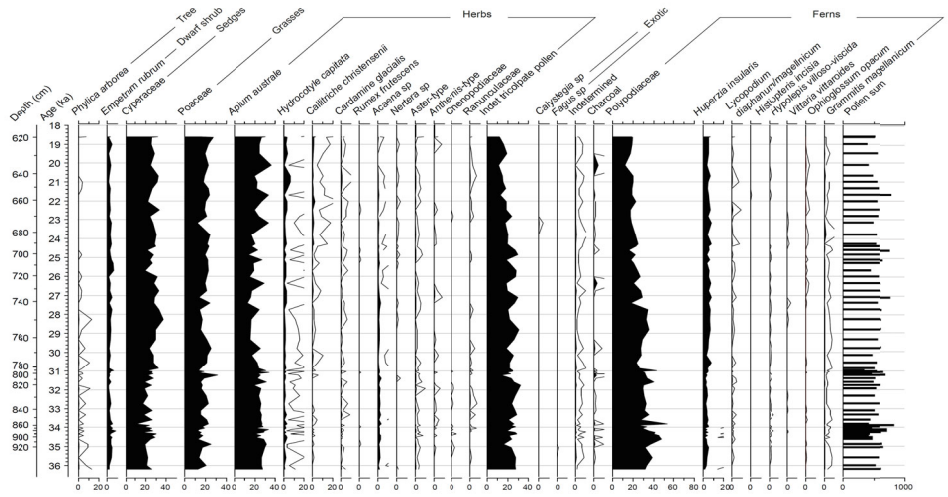

Figure 5. Pollen diagram from 1st Pond, Nightingale Island. The diagram shows relative abundance (%) of the pollen taxa. Note that it is both related to depth (cm) and age (ka) on the y-axis, the latter according to the age-depth model in Fig. 3.

432 To evaluate changes in the degree of weathered material we used a modified
433 Chemical Index of Alteration (CIA) (Fig. 4D). The long-term development can be divided
434 into three phases with initially low but very variable values until 31 ka, a second phase with
435 stable intermediate CIA values until 27 ka, followed by higher and varying values (Fig. 4D).
436 Magnetic susceptibility (MS) shows centennial-millennial oscillations superimposed on an
437 increasing trend from the bottom to the top of the core (Fig. 4M), and is an indicator of in-
448 washed mineral matter from magnetite-rich basaltic rocks of the catchment. The values of
449 total organic carbon (TOC) and biogenic silica (BSi) (Figs. 4L and J) reflect organic and

aquatic productivity in and around the lake with highest values in the oldest section. TOC shows a general decline and BSi oscillates with higher values until 28 ka, after which it gradually drops. The fairly high C/N ratios (Fig. 4K), with a mean value of 17.6, show that organic matter is a mix of terrestrial and aquatic sources. The high and oscillating ratios in the older section followed by a gradual decline implies terrestrial sources dominating until 28 ka, after which time aquatic sources become more important. With respect to bulk stable isotopes (Fig. S1), the high $\delta^{15}N$ values imply a marine influence~~origin~~ possibly related to presence of marine birds (Caut et al., 2012), such as Great Shearwater and Albatrosses which have a great impact on the Ponds today~~, suggesting a more or less continuous impact of SHW~~. Rising $\delta^{13}C$ values at 25.7 ka are consistent with the declining C/N ratios after 28 ka, i.e. more aquatic material with enriched ^{13}C, and perhaps~~possibly~~ in combination with higher influence from C_4 grasses.

Unlike the pollen record (Fig. 5), the diatom record shows large shifts and the 33 diatom taxa (Fig. S2) have been classified into three environmental forms. Changes in these groups imply shifts in aquatic and environmental conditions in and around the lake. They show a lake with open water early in the record, followed by shifting lake levels between 35-33 ka (Fig. 4I), supported by δD values of long- and mid-chain *n*-alkanes (Fig. 4F). At 31 ka the open water ratios drop and reach a minimum at 29 ka, in anti-phase with the acid water diatom ratios (Fig. 4G), followed by a rise until 26.6 ka. Thereafter acid species dominate, as oligotrophic wetland encroached around the lake, while periods of more terrestrial diatoms imply episodes of in-washed diatoms from the surroundings. Around 21.2 ka more open water conditions prevail again with high ratios 19-18.6 ka, before the lake dried out (Ljung et al., 2015). The shifts in diatom communities shows that 1P went through substantial hydrologic changes, some of which were rapid, induced by changing P/E ratios, in contrast to the fairly stable vegetation around the lake as seen in the pollen record.

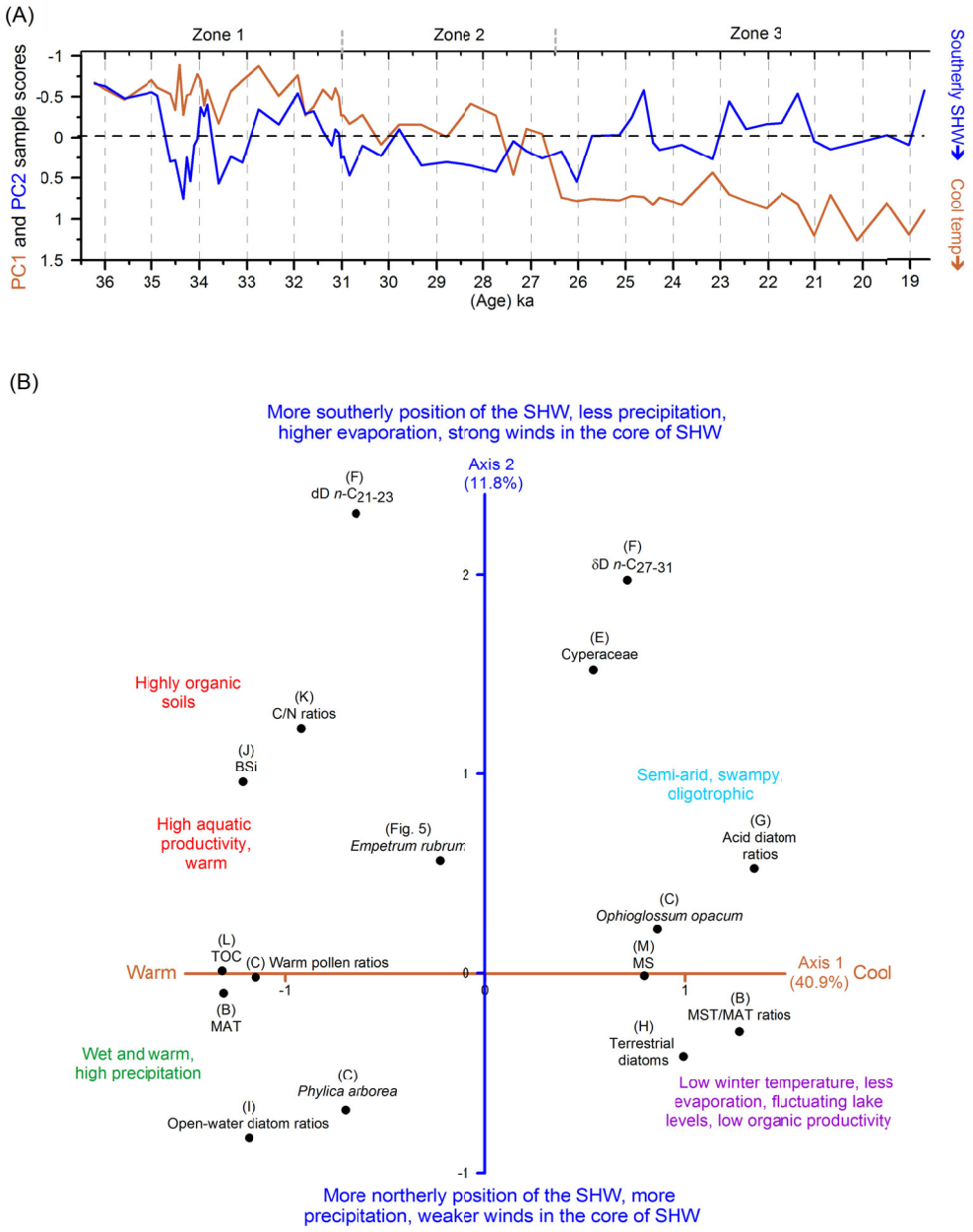

Figure 6. Principal Ceomponent ~~a~~Analysis (PCA) of 16 proxies from 1st Pond. (A) Scores of the first two principal components related to age and the three PCA zones. Note that negative values point upwards and how PC1 and PC2 values relate to temperatures and SHW to the right y-axis. (B) PCA plot shows the loadings of the 1~~6~~4 proxies (shown as red~~black~~ dots and black text with reference to proxies in Fig. 4, except for *Empetrum rubrum*). PC1 (red brown) and PC2 (blue) accounts for 38.1~~40.9~~ and 13.4~~11.8~~% of the variance, respectively. The interpretations of the two axes are shown by red brown and blue texts, and the interpretations of the four segments are based on the combined positions of the proxies in the plot, and are shown in four different colors. ~~MST/MAT=mean summer temperature/mean annual temperature, i.e. a proxy for low winter temperatures.~~

4.2 Linking the Nightingale Island record to South Atlantic hydroclimate

The hydrological sensitivity of a basin like 1P makes it ideal to place local changes into the context of regional hydroclimate shifts. To analyze the variability through time Principal Component Analysis (PCA) was carried out on a data set with 146 hydroclimate-sensitive proxies resulting in 3 PCA zones (Fig. 6A). Note that resolution of the PCA record depends on the proxy with least common sample levels (Table S2), in this case biomarker analyzes. Therefore the temporal resolution of the PCA is not as high as some ice core and marine records. Based on the proxy loadings in the PCA plot (Fig. 6B), it can be divided into four different segments with variable hydroclimate and environmental conditions. The importance of presumed temperature proxies on Axis 1 (38.140.9% of the variance) is evident ~~obvious~~ where ~~reconstructed MAT,~~ warm pollen ratios, *Phylica arborea* pollen, BSi, TOC and open-water diatoms show warm humid conditions to the left (negative) in the biplot (Fig. 6B), vs cooler and drier to the right. The latter is accentuated by *Ophioglossum* spores, a fern growing at high and cold altitudes on TdC~~, and colder winter temperatures implied by the MST/MAT ratio~~. A correlation analysis between the PC1 values and our MAAT values (Fig. 4B) shows an r^2 value of 0.56, corroborating that Axis 1 mainly represents temperature. Axis 2 (13.41.8% of the variance) is linked to hydrologic indicators being dominated by the δD values of the aquatic *n*-C_{21-23} and terrestrial *n*-C_{27-31} alkanes (Fig. 6B). We interpret higher δD values (positive axis 2 values) to show stronger influence of more local air masses, with more evaporation and semi-arid conditions, also shown by *Empetrum rubrum* pollen in the upper left quadrant, while the upper right quadrant of the plot shows an acid oligotrophic swampy setting. The segment to the lower right in Figure 6B displays cold conditions and in-wash of terrestrial diatoms as an effect of higher lake level during episodes of more precipitation. The lower left represents warm and wet conditions, implied by *P. arborea* pollen and open water diatoms, and in general, negative axis 2 values relate to more negative δD values.

Formaterat: Upphöjd

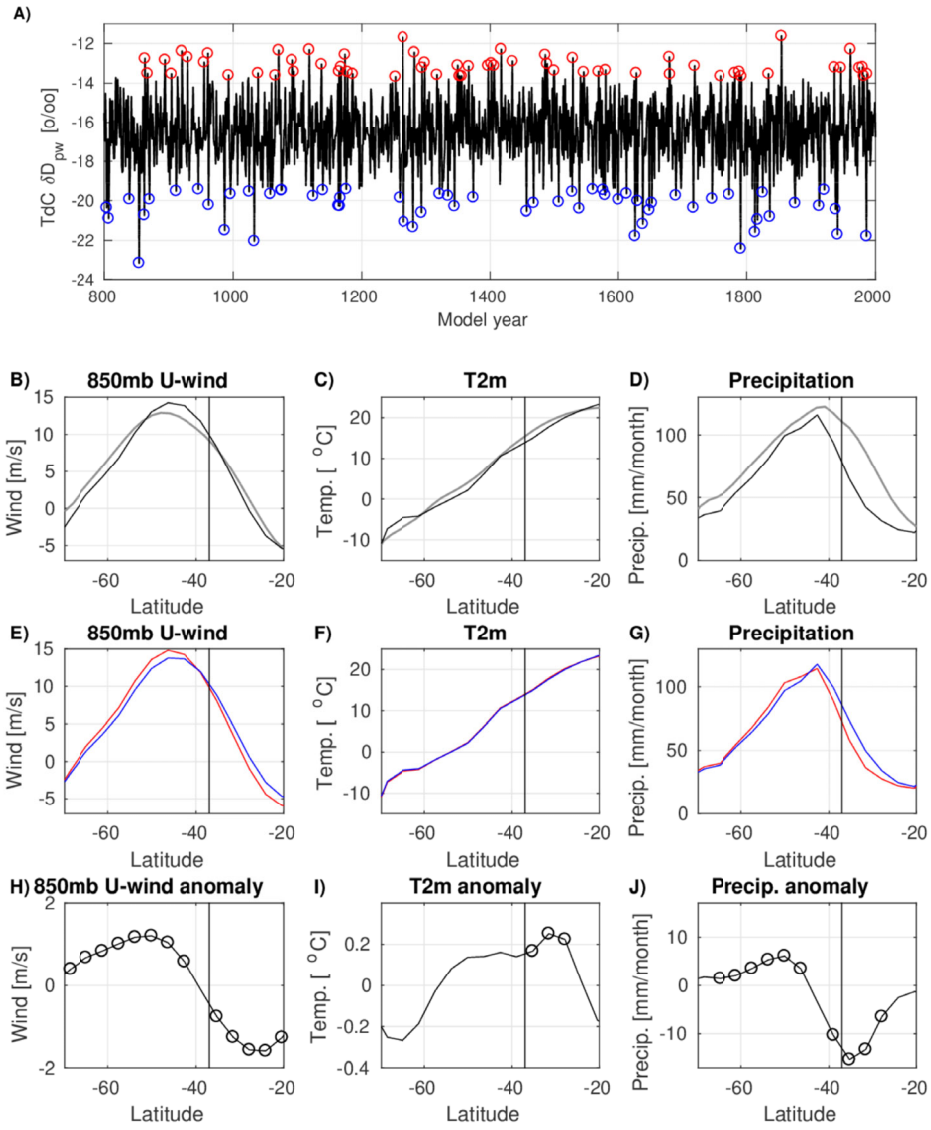

Figure 7. Zonal mean changes in wind, temperature and precipitation related to δD variability at TdC. A) Time series of simulated precipitation weighted annual mean δD at TdC, with values above and below the 95th percentile indicated with red and blue circles, respectively. This selection of high and low δD is used to define the data in figures E-G. (B-D) Annual modeled (black) South Atlantic zonal mean (30°W to 0°W) westerly wind speed (850mb U-wind, positive towards east), 2m temperature (t2m) and precipitation compared to the 20th Century Reanalysis climatology 1981-2010 (gray) (Compo et al., 2011). (E-G) Composites of annual modeled zonal mean (30°W to 0°W) westerly wind

514 speed (850mb U-wind), 2m temperature (t2m) and precipitation for high (red) and low (blue) δD at
515 TdC defined in (A). (H-J) High-minus-low anomalies of model output are shown in (E-F). Circles
516 indicate significant anomalies ($p < 0.01$) calculated using two-tailed Student's t-test. The vertical bars
517 in (B-J) show the latitude of NI at 37°S.

518 ~~Observations of the isotopic content of precipitation are very sparse around TdC.~~
519 ~~Therefore we have investigated the hydroclimate variability with an isotope enabled climate~~
520 ~~model.~~ To illustrate the relation between the position of the westerlies and the isotopic
521 composition of precipitation at TdC in the simulation, we selected extreme values of high and
522 low δD at TdC (Fig. 7A), and made composite anomalies of the annual mean westerly wind
523 strength at 850mb (u850mb, Fig. 7A), precipitation (Fig. 7B), 2m temperature (t2m, Fig. 7C)
524 and precipitation weighted δD (Fig. 7D) for high-minus-low δD at TdC. This shows that the
525 variability of δD in precipitation at TdC is only weakly dependent on local temperature.
526 Instead, shifts in δD at TdC are related to large scale changes in precipitation and the position
527 of the westerlies. Positive δD anomalies at TdC imply a more southern position of the core of
528 the westerlies with drier and more subtropical conditions at TdC, and negative δD anomalies
529 at TdC denote a more northern position of the core of the westerlies bringing more polar air
530 masses with wetter conditions at TdC. From Figs. 7 and 8, we note that the shifts in TdC
531 precipitation are governed by the precipitation zone on the northern flank of the westerlies
532 shifting with the position of the westerlies themselves. We therefore conclude that our model
533 analysis shows that isotope variability in precipitation at TdC is mainly related to shifts in
534 large scale circulation. High δD values at TdC imply a more southerly SHW position with
535 stronger winds in its core, while low δD values show a more northerly SHW position with
536 weaker winds (Figs. 7E and H). Our analysis also shows that high (low) δD values are related
537 to less (more) precipitation at TdC, but shows little dependency on temperature (Figs. 7F and
538 I, and 8C). The amplitudes of the δD values in our proxies are significantly larger than the
539 modelled amplitudes, implying larger changes in the climate variables during the recorded
540 isotope shifts compared to the year-to-year variability of the model. Furthermore, ~~T~~the
541 modelled relationship between δD and precipitation corresponds well to the PC2 variability of

the proxies (Fig. 6B); for example high PC2 and δD values relate to more Cyperaceae (lake overgrowth) and *Empetrum* pollen values (arid soils) and more acid diatoms (swampy), while low PC2 values relate to open-water (lake) and terrestrial (flushed-in) diatoms.

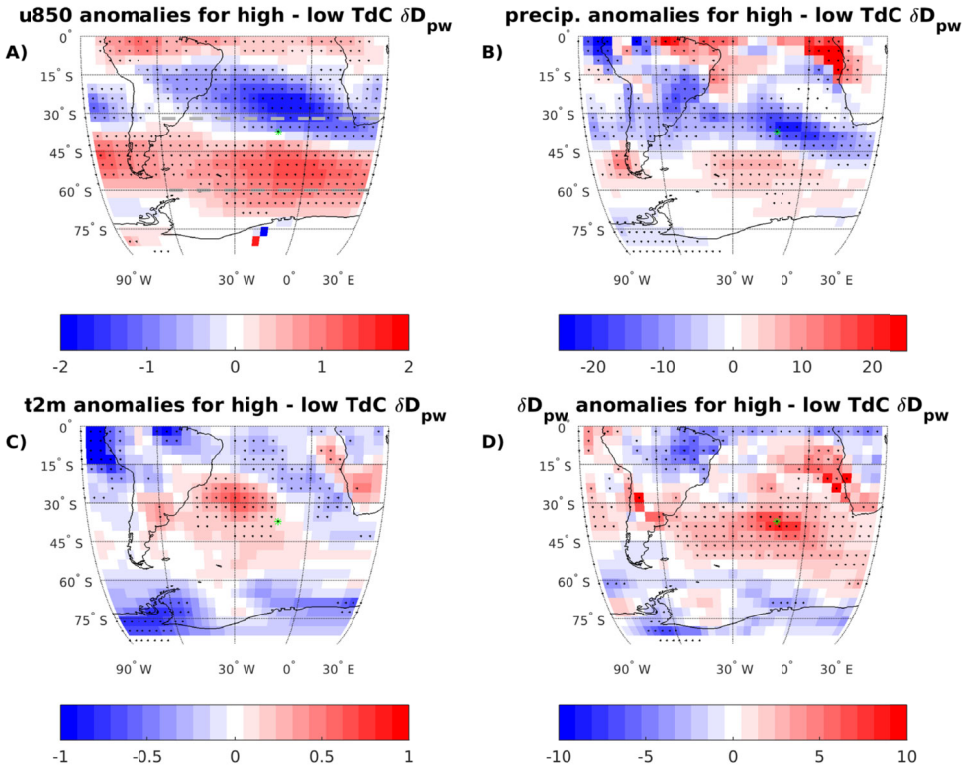

Figure 8. Composite maps of changes in wind, precipitation, temperature and δD related to δD variability at TdC, showing annual anomalies based on composites for high and low δD at TdC (see Figure 7A). A) Westerly wind speed (850mb U-wind, positive towards east, [m/s]). The dashed gray lines show the approximate northern and southern boundaries of the westerlies (850mb U-wind > 5 m/s) to clarify that high TdC δD is related to a southward shift in the westerlies. B) Precipitation [mm/month]. C) 2m temperature (t2m, [°C]). D) precipitation weighted δD [‰]. Stippling indicates significant anomalies ($p < 0.01$) calculated using a two-tailed Student's t-test. The green spot shows the position of TdC.

5 Hydroclimate correlations and interpretations

5.1 The large-scale hydroclimate pattern

The three PCA zones displayed in Figures 6A and 9, dated to 36.2-31.0, 31.0-26.5 and 26.5-18.6 ka, show a trend and pattern which is recognizable in much of our data set as well as in

the EDML (Fig. 4A) and South Atlantic marine record (Fig. 10B). Zone 1 is fairly warm but oscillates between low and high PC2 values, related to more northerly and weaker SHW, and more local air masses with stronger westerlies in a more southern position, respectively. Zone 2 is generally more stable with some minor oscillations with more southerly SHW and corresponds largely to the fairly warm period in Antarctica with the three isotope maxima AIM4.1, AIM4 and AIM3 (Fig. 4A), and a stable and mild period in the South Atlantic marine realm (Fig. 10B). Zone 3 shows a cooling trend, also visible in the EDML and marine record, with variable SHWs. It appears that TdC was continuously influenced by the SHW, as shown by the absence of arid conditions and generally low δD values, verified by humid conditions in southwestern-most Africa throughout most of MIS3 and MIS2 (Chase and Meadows, 2007). Apart from the resemblance between the long-term trends in Antarctic ice core data and marine data at 41°S in the South Atlantic (Barker and Diz, 2014) with our data it is, in spite of our lower resolution, interesting to compare our PC2 and δDn-$C_{C27-C31}$ records (Figs. 4A and 10G) with other regional records related to SHWs. Taking age uncertainties of a few hundred years into account we note a resemblance with marine Fe fluxes at 42°S (Martínez-García et al., 2014) where low δD values (Fig. 10G) co-vary with high Fe fluxes (Fig. 10F) due to northerly SHW in a cooler Southern Hemisphere, thus expanding the Patagonian dust source. Similar co-variability can be seen in the $\delta^{18}O$ record on fluid inclusions of SE Brazilian speleothems (Millo et al., 2017) where low values (Fig. 10E) imply strengthening of the monsoon shifting the South Atlantic atmospheric system southwards, including SHW. We also note that the Antarctic CO_2 record (Fig. 10C) and the [CO_3^{2-}] record (Gottschalk et al., 2015) from the South Atlantic (Fig. 10D), inferring AMOC strength and Southern Ocean ventilation, share similarities with our SHW records, ~~as~~ described in the section below.

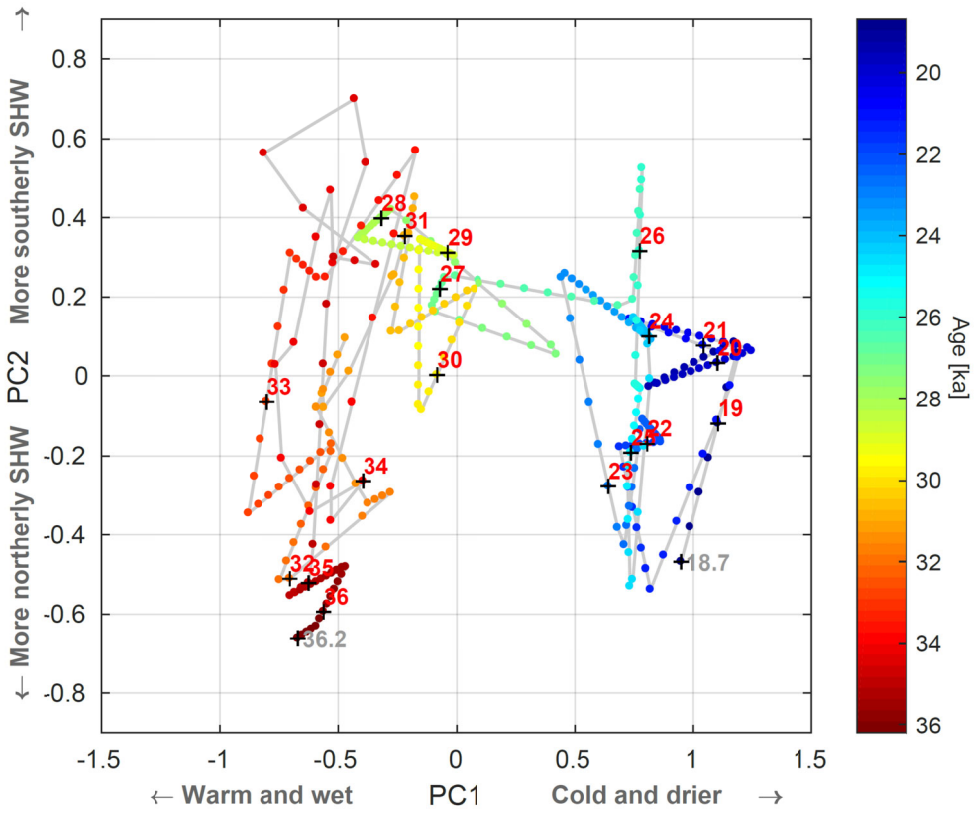

Figure 9. Parametric plot of the PC1 and PC2 sample values as a function of time shown by the color bar to the right. Red numbers denote each ka with grey numbers at the start and end of the plot. Data was interpolated to 50-year time steps to illustrate rate of change; the larger distance between dots the more rapid change. Note that the hydroclimate interpretations from Figure 6B are shown on the two PC axes.

5.2 A detailed hydroclimate scenario for the central South Atlantic

Due to chronological uncertainties in all records, lower resolution in some records and the complex phase-relationships during abrupt interhemispheric climate shifts (Markle et al., 2016), detailed comparison of short-term variations across sites has to be treated with caution. In spite of these short-comings we will present a scenario based on our record and likely correlations.

The start of our record shows warm and wet conditions with northerly SHW, coinciding with the long and warm AIM7 followed by a cooling (Fig. 10J) at the onset of

598 DO7. This is followed by the very dynamic period 35-33 ka, shown by high sedimentation
599 rates (Fig. 3) and peak variability in terms of both rapidity and amplitude (Fig. 9). Such
600 variability is also seen in marine and ice core records, and in spite of the age uncertainties at
601 34-35 ka (Fig. 3) we tentatively correlate this period in our record to the end of DO7 and the
602 minimum between AIM6 and AIM7. This corroborates the overlaps and time lags that have
603 between postulated for DO and AIM events (Markle et al., 2016; Pedro et al., 2018; WAIS
604 Divide Project Members, 2015). At 34 ka we note a temperature peak at the onset of AIM6
605 (Figs. 4 and 11) followed by falling temperatures, δD, Fe flux and CO_2 values and high
606 humidity (Figs. 10G, F, C and H). This change reflects northerly and weaker westerlies, with
607 rising speleothem $\delta^{18}O$ and WAIS d_{ln} values (Figs. 10E and 11E), denoting the start of DO6
608 with a warming of the NH (Fig. 10A). This caused northwards shifting ITCZ and SHW in line
609 with the theory that the atmospheric circulation system moves towards the warmer
610 hemisphere, responding to the change in the cross-equatorial temperature gradient (McGee et
611 al., 2014). At 33.5 ka we see a southward SHW shift with rising temperatures and higher CO_2
612 and lower WAIS d_{ln} values with dry conditions. We relate this to the onset of AIM5; a
613 warming which is interrupted at 32.8 ka by a northerly SHW shift and wetter conditions (Figs.
614 11F and 10H) possibly triggered by DO5. This partly continues until 31.7 ka when SHW
615 moves south with a minor temperature rise (Fig. 11D) and decreasing humidity, possibly as a
616 response to the post-DO5 cooling (Fig. 10A). The high variability and large amplitude of the
617 changes of Zone 1 (Fig. 9) have facilitated conceivable correlations to other records. Based on
618 these we can conclude that at large, PC2 implies northerly shift of the SHW during warm
619 North Atlantic periods, and a more southerly position during warm periods in Antarctica, also
620 in line with interpretation of Antarctic deuterium excess data (Markle et al., 2016).

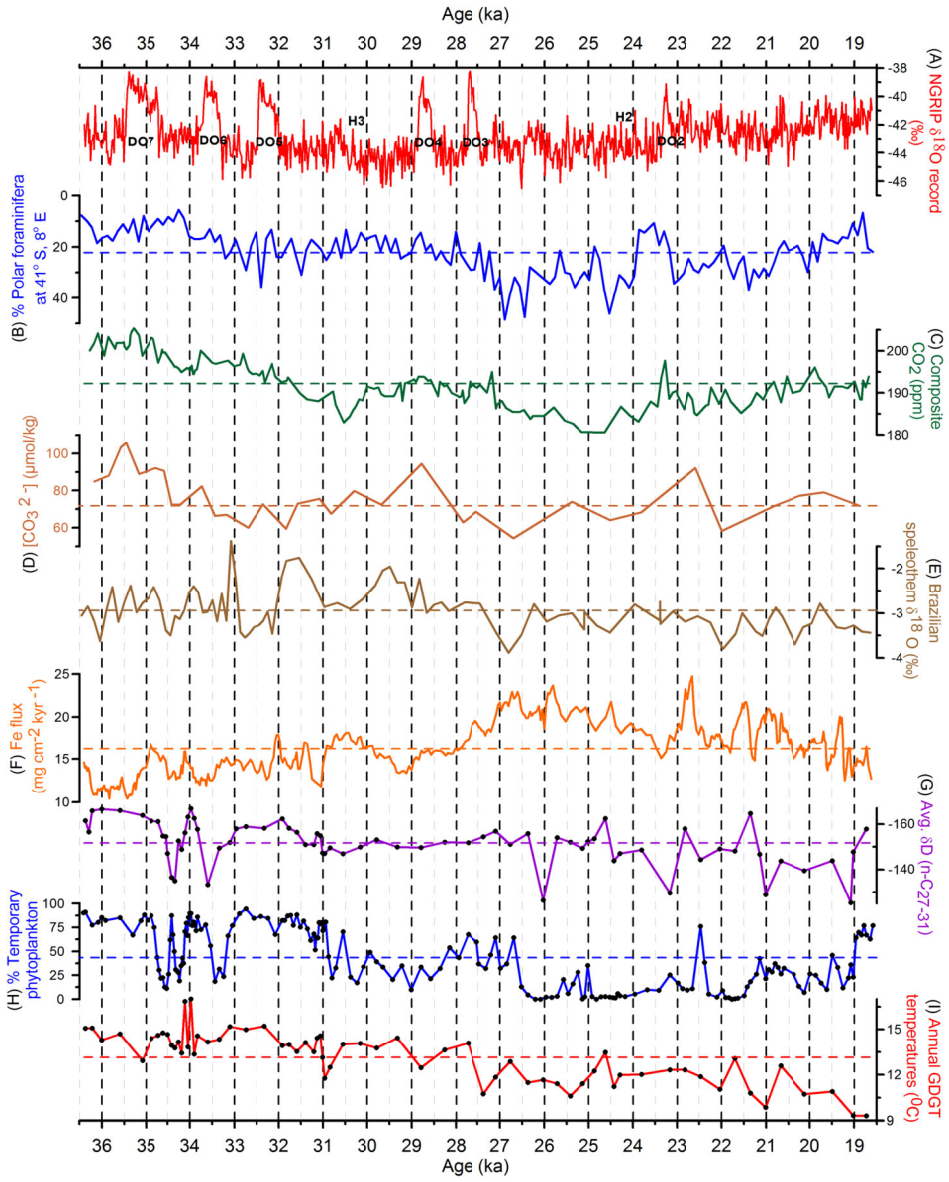

Figure 10. Comparisons between other proxy records (A-F) and Nightingale Island proxies for SHW (G), wetness (H) and temperature (I), with mean values as broken lines. (A) $\delta^{18}O$ values from the NGRIP ice core (Andersen et al., 2006) showing DO and H events. Ice core records are on a common time scale (Veres et al., 2013). (B) Abundance (%) of polar foraminifera at 41°S in the S Atlantic (Barker and Diz, 2014). (C) Composite Antarctic CO_2 record from Siple Dome (Ahn and Brook, 2014) and WAIS (Stenni et al., 2010). (D) $[CO_3^{-2}]$ data at 44°S in the South Atlantic (Gottschalk et al., 2015). (E) Speleothem ^{18}O record on fluid inclusions from SE Brazil (Millo et al., 2017). (F) Fe flux data in the South Atlantic at 42°S (Martínez-García et al., 2014). Then follow NI data, (G) Average δD values for the terrestrial *n*-C_{27-31} alkanes. (H) Abundance (%) of temporary phytoplanktonic diatoms implying relative water depth. (I) Annual NI temperatures from the GDGT analyses. Note that that sample levels are shown by a dot in (G)-(I) and that y-axes of (B) and (G) show higher values downwards to

facilitate comparisons to other proxies. Note that the two thick gray lines (31 ka and 26.5 ka) indicate the position of the three PCA zones (Fig. 6).

The Zone 1/Zone 2 boundary at 31 ka (Fig. 6A) is a dynamic transition, shown by many proxies and peak sedimentation rates (Figs. 9 and 3). The 4.5 ka long and stable Zone 2 (Fig. 6A) is characterized by fairly high but slightly decreasing temperatures and as in Zone 1 a dominating southerly SHW position. It is possible, taking age uncertainties into account, that H3 at 30.5 ka (Fig. 10A) triggered the southbound SHW, ~~and~~ the rising CO_2 and ~~MAT~~MAAT values, and the reduced humidity between 31-30 ka (Figs. 11F, 10C, 10I and 10H). The following long and warm AIM4 may have stabilized conditions in the South Atlantic in spite of the DO4 event at 28.8 ka. This stability is also seen in marine records (Fig. 10B), and the rather stable southern position of the SHW agrees with the fairly high CO_2 values between 30-27.2 ka and with falling and rather low Fe fluxes (Fig. 10F). We also note higher lake evaporation from δD values of the aquatic *n*-C_{23} (Fig. 4F), in concert with rising summer insolation (Fig. 11A). Around 27.5 ka we see a brief response in some of the proxies to the short DO3 event (Fig. 10A), such as the ~~MAT~~MAAT and PC2 records (Figs. 11D and F), which~~and~~ is also noticeable in e.g. the marine and Brazilian monsoon records (Figs. 10B and E).

The start of Zone 3 at 26.5 ka (727 cm) constitutes the most drastic change in our record (Figs. 6A and 9) but timing varies between proxies (Fig. 4). ~~MAT~~MAAT, TOC and C/N ratios start to decrease already at 28 -27.5 ka, coinciding with DO3, while the biologic proxies (Figs. 4C and G-J, Fig. S2) respond slightly later possibly because they do not react until certain hydroclimate thresholds for the vegetation and algae flora are reached. The Zone 2-3 transition is roughly simultaneous with the onset of LGM in Antarctica (Fig. 10C), when 1P switched from a lake to a wetland, coinciding with increased abundance of polar foraminifera at 41°S (Fig. 10B). This may be an effect of the STF moving north of TdC, a meridional shift comparable to what has been shown from the eastern Pacific (Kaiser et al.,

2005). The fairly stable PC1 values show cool and less humid LGM conditions, while the variable PC2 values imply shifts in the position of SHW (Fig. 11F). There is also ~~a good~~ some correspondence between our δD (n-C_{27-31}) maxima after 27 ka and Fe flux minima from the South Atlantic (Figs. 10G-F), both indicating southerly shifts of SHW. During this period our data also show generally higher mean δD (n-C_{27-31}) values than in Zone 1, implying a more southern position of SHW during the Antarctic LGM, as seen in some modeling results (e.g. Sime et al., 2016). This is also compatible with the fact that the LGM temperature lowering in the Northern Hemisphere (Johnsen et al., 1995) was much larger than in the south (Stenni et al., 2010), shifting the atmospheric system to the south due to changes in the cross-equatorial gradient (McGee et al., 2014), also~~as~~ implied by the speleothem $\delta^{18}O$ data (Fig. 10E) showing increased precipitation (Millo et al., 2017).

After 26.5 ka we note phases of less humid swampy oligotrophic conditions on NI at 26, 24.5-23, 22 and 20.5-19 ka (Fig. 10H) interrupted by periods of more or less open water, possibly driven by shifts of SHW. The former often show enriched δD values (Fig. 10G), while the latter were characterized by higher precipitation and more depleted δD values. Regarding the response of CO_2 to these SHW shifts we note a fairly good agreement between low/falling CO_2 values and a northerly SHW position, and vice versa. For example, the CO_2 minimum at 24.5-25 ka (Fig. 10C) matches with an extreme northern SHW position (Figs. 10G and 11F), and the CO_2 peak at 23.3 ka agrees with the end of a long phase of southwards moving SHW. The latter might have been triggered by the onset of H2 at 24.1 ka (Fig. 10A) followed by the inception of AIM2 (Fig. 11C).

The absence of *P. arborea* (Figs. 4C and 5) and our temperature proxies (Fig. 4B) imply that minimum winter temperatures at our site were occasionally below zero, especially after 26 ka; periods of frost also explain increased mechanical weathering (Fig. 4D). Between 23 and 19 ka the Antarctic winter sea ice reached 47°S in the South Atlantic

(Gersonde et al., 2005), only some 1000 km south of TdC. Our 1P record shows a declining temperature trend during the end of this period (Fig. 10I), in contrast to rising temperatures in Antarctica and South Atlantic (Figs. 11C and 10B). This regional temperature anomaly may be explained by the declining summer insolation at the latitude of Tristan da Cunha (Fig. 11A), and may also, at the end of LGM, be related to break-up of Antarctic ice shelves as sea levels rose, causing cooler conditions further north. In fact, temperature minima after 19 ka are seen in both our record and in marine data (Figs. 10I and B), as well as a δD minimum (Fig. 10G).

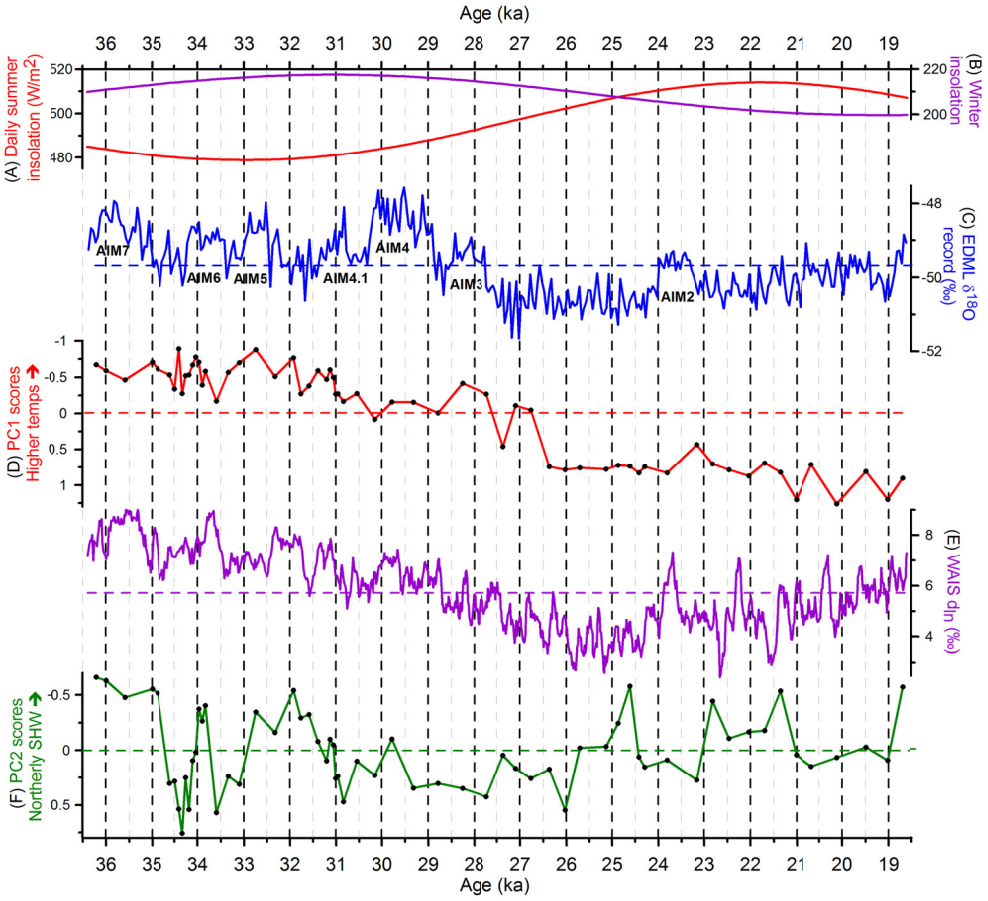

Figure 11. Comparison between our PC1 and PC2 records and other relevant data. **(**A and B**)** Mean daily summer and winter insolation at 37°S (Laskar et al., 2004). (C) EDML $\delta^{18}O$ record (EPICA Community Members et al., 2006) with Antarctic Isotope Maxima (AIM). (D) PC1 scores implying

temperature shifts at NI. (E) WAIS d_{ln} values from west Antarctica (Markle et al., 2016). (F) PC2 scores indicate impact of SHW at NI. Note that sample levels, i.e. time resolution, for the PC records are shown as dots. Note that the two thick gray lines (31 ka and 26.5 ka) indicate the position of the three PCA zones (Fig. 6).

5.3 A climate synthesis

In general, our data implies two main climate modes for the study period, separated by a transition period 31-26.5 ka, Zone 2. This is displayed in Figure 9, with pre-LGM (Zone 1) clearly separated from the LGM period (Zone 3) on Axis 1, but also with higher variability of the pre-LGM period. This variability is possibly related to an active bipolar seesaw mechanism during Zone1/MIS3 even at the fairly low latitudes of TdC, triggering N-S shifts of SHW and related hydroclimate conditions. Any CO_2 effects from the rapid SHW shifts in Zone 1 are not discernible, but the dominating more northern SHW position may have resulted in the general CO_2 decline (Fig. 10C). With the onset of Zone 2 there may be a stronger link between CO_2 and SHWs. In view of carbon-cycle time lags, the mainly southerly positioned and more intense SHW at 31-27.5 ka (Fig. 11F) may have resulted in the rising and higher CO_2 concentrations at 30.5-27.2 ka (Fig. 10C), with more upwelling, CO_2 outgassing and less sea ice. The LGM mode is characterized by falling and low temperatures, lack of clear effects of the bipolar seesaw mechanism, possibly due to the much stronger cooling in the north as the cross-equatorial gradient changed. The variability is mainly related to proxies associated with SHW changes, as summarized by PC2, with a similarly high frequency variability of WAIS d_{ln} and Fe fluxes (Figs. 11E, 10F), with resulting CO_2 variability. However, a key difference between our SHW proxies (PC2) and the WAIS d_{ln} record is that the latter represents SHW variability superimposed on large scale temperature trends while our PC2 record reflects the SHW signal without temperature impact.

Thus, the largest change in our record occurs after 27.5 ka when the effects of the strong post-DO3 cooling of the Northern Hemisphere start dominating the hydroclimate of the South Atlantic with highly variable SHW after 25 ka ; possibly a prerequisite for the oscillating CO_2 levels after the CO_2 minimum at 25 ka (Fig. 10C).

6. Conclusions

In conclusion, we think our Nightingale Island data demonstrates the potential for remote island proxy records to register large scale atmospheric shifts in an oceanic setting, especially if the island location, in relation to marine and atmospheric fronts, is well-chosen. In addition, if the right types of proxies are chosen, multiproxy lake records have a particularly large potential, since they disclose both terrestrial and aquatic responses to shifting atmospheric conditions, as shown in our 1P record. By combining these responses they can be translated into relative changes in hydroclimate conditions.

Our 1P data~~, reflecting terrestrial and aquatic responses to shifting atmospheric conditions,~~ show that the glacial hydroclimate of South Atlantic mid-latitudes experienced varying degrees of humidity, but with more or less continuous impact of SHW. Temperature conditions were in general warm but oscillating during MIS3, with shifting strength and positions of the westerlies. Weaker and northwards moving SHW at the onset of NH interstadials with stronger and southerly westerlies during NH stadials partly reflect the complex processes behind phase relationships between Greenland and Antarctic ice core climate records (Pedro et al., 2018). These shifts, possibly triggered by changes in the cross-equatorial gradient, are to some extent manifested by rising (falling) CO_2 levels when SHW was stronger (weaker) and located more towards the south (north), in line with Holocene records (Saunders et al., 2018). The largest variability in our record is seen during the fairly warm and humid period 36.5-31 ka with frequent and abrupt shifts, followed by a fairly stable period 31-27 ka with slowly declining temperatures and dominating southerly SHWs. The

Formaterat: Teckensnitt:(Standard) Times New Roman

largest over-all change occurs after 27 ka , exhibited by a distinct cooling trend. This early mid-latitude cooling is in phase with LGM in Antarctica, consistent with some modeling results (Fogwill et al., 2015). We think this represents a mode shift in hydroclimate; from the highly variable MIS3 conditions through the more steady conditions 31-27 ka (Figs. 11D and F) into LGM with its cool and less humid climate, perhaps as a result of the SF moving north of TdC. The variable position of SHW (Fig. 11F), with particularly high δD values at 26, 23.1, 21 and 19.1 ka (Fig. 10G), is noteworthy, inferring fairly sudden and distinct southerly shifts of the westerlies. The end of our record shows that fairly cool conditions persisted in these SH mid-latitudes until at least 18.6 -ka. This might have been a combined effect of declining summer insolation and northward shifting westerlies (Figs. 11A and F), conveying cold air masses, sea ice and ice bergs far north ~~from~~of Weber et al.´s (2014) first peak of iceberg-rafted debris from collapsing Antarctic ice shelves starting at 20 ka, and named MWP-19KA. ~~(Weber et al., 2014).~~

Author contributions. S.B. was the initiator of the study, received funds, drilled and described cores, carried out sampling and XRF analyses and contributed with most writing, J.S. contributed with interpreting data, much writing, ran the isotope model experiment (ECHAM5-wiso/MPI-OM) and analyzed all modeling results, K.L. drilled and described cores, carried out sampling, analyzed C, N, ^{13}C, ^{15}N, pollen and contributed with writing, F.A contributed with the age model and some writing, R.F. contributed with interpreting and analyzing diatom results and some writing, R.H.S. helped interpret biomarkers and hydrogen isotopes and contributed with some writing, M.E.K. analyzed XRF results and contributed with some writing, T.F.S. contributed with creative inputs and some writing, S.H. sampled and carried out diatom analyzes, H.J. carried out multivariate statistics, Y.K.K.A. analyzed biomarkers and hydrogen isotopes, R.M. calculated insolation values and contributed with little writing, J.E.R. carried out biomarker analyses and calibrated the GDGTs and N.V.d.P, carried out biogenic silica analysis. All commented on the manuscript.

Acknowledgements. The co- members of the 2010 Tristan expedition (M. Björck, A. Björk, A. Cronholm, J. Haile, M. Grignon) and Tristan islanders are gratefully acknowledged for hard work at sea and on Nightingale I. The isotope enabled climate model, ECHAM5-wiso/MPI-OM, was run at the AWI Computer and Data Center. We thank M. Werner for helping to set up and run the model simulations, S. Barker, F. Cruz and C. Millo for providing us with their data, G. Ahlberg for pollen sample preparations and Å. Wallin for magnetic susceptibility measurements. We are grateful for financial support, incl. expedition costs, from the Swedish Research Council (VR), the Crafoord Foundation, the Royal Fysiographic Society, the LUCCI Centre in Lund and the Lund and Stockholm

783 universities. We dedicate this paper to Charles T. Porter, our skipper on his ketch Ocean Tramp, who
784 challenged all kind of weather in the South Atlantic to retrieve our unique sediment cores. However,
785 he sadly died suddenly in March 2014 while preparing for our next expedition: a great loss in many
786 respects but mostly as an invaluable, memorable friend and colleague.

787

788

789

790

791

792

793

794

795 # References

796

797 Ahn, J. and Brook, E. J.: Siple Dome ice reveals two modes of millennial CO2 change during the last
798 ice age, Nat. Commun., 5, 3723, 2014.

799 Andersen, K. K., Svensson, A., Johnsen, S., Rasmussen, S. O., Bigler, M., Röthlisberger, R., Ruth, U.,
800 Siggaard-Andersen, M. L., Steffensen, J. P., Dahl-Jensen, D., Vinther, B. M. and Clausen, H. B.: The
801 Greenland Ice Core Chronology 2005, 15-42 ka. Part 1: Constructing the time scale, Quarternary Sci.
802 Rev. 25, 3246–3257, doi:https://doi.org/10.1016/j.quascirev.2006.08.002, 2006.

803 Anker Björk, A., Björck, S., Cronholm, A., Haile, J., Ljung, K. and Porter, C.: Possible Late
804 Pleistocene volcanic activity on Nightingale Island, South Atlantic ocean, based on geoelectrical
805 resistivity measurements, sediment corings and ^{14}C dating, GFF, 133, 10.1080/11035897.2011.618275,
806 2011.

807 Bard, E. and Rickaby, R. E. M.: Migration of the subtropical front as a modulator of glacial climate,
808 Nature, 460, 380–383, doi:10.1038/nature08189, 2009.

809 Barker, S. and Diz, P.: Timing of the descent into the last Ice Age determined by the bipolar seesaw,
810 Paleoceanography, 29, 489–507, doi:10.1002/2014PA002623, 2014.

811 Battarbee, R. W. and Keen, M. J.: The use of electronically counted microspheres in absolute diatom
812 analysis, Limnol. Oceanogr., 27, 184–188, 1982.

Battarbee, R. W., Jones, V. J., Flower, R. J., Cameron, N. G., Bennion, H., Carvalho, L. and Juggins, S.: in Diatoms, 155–202, Kluwer Academic Publishers, Dordrecht., 2001.

Berglund, B. E. and Ralska-Jasiewiczowa, M.: Pollen analysis and pollen diagrams, in Handbook of palaeoecology and palaeohydrology, edited by B. E. Berglund, 455–484, John Wiley and sons, Chichester., 1986.

Broecker, W. S.: Paleocean circulation during the Last Deglaciation: A bipolar seesaw?, Paleoceanography, 13, 119-121, doi:199810.1029/97PA03707, 1998.

Bronk Ramsey, C.: Radiocarbon Calibration and Analysis of Stratigraphy: The OxCal Program, Radiocarbon, 37, 425–430, doi:10.1017/S0033822200030903, 1995.

Bronk Ramsey, C.: Deposition models for chronological records. Quaternary Sci. Rev., 27, 42-60, 2008.

Bronk Ramsey, C.: Bayesian Analysis of Radiocarbon Dates, Radiocarbon, 51, 337–360, doi:10.1017/S0033822200033865, 2009a.

Bronk Ramsey, C.: Dealing with Outliers and Offsets in Radiocarbon Dating, Radiocarbon, 51, 1023–1045, doi:10.1017/S0033822200034093, 2009b.

Caut, S., Angulo, E., Pisanu, B., Ruffino, L., Faulquier, L., Lorvelec, O., Chapuis, J-L., Pascal, M. Vidal, E. Courchamp, F. Seabird modulation of isotopic nitrogen on islands. PLoS ONE 7:6, e39125, 2012.

Ceppi, P., Hwang, Y.-T., Liu, X., Frierson, D. M. W. and Hartmann, D. L.: The relationship between the ITCZ and the Southern Hemispheric eddy-driven jet, J. Geophys. Res. Atmos., 118, 5136–5146, doi:10.1002/jgrd.50461, 2013.

Chase, B. M. and Meadows, M. E.: Late Quaternary dynamics of southern Africa's winter rainfall zone, Earth Sci. Rev., 84, 103–138, doi:10.1016/j.earscirev.2007.06.002, 2007.

Chiang, J. C. H., Lee, S.-Y., Putnam, A. E. and Wang, X.: South Pacific Split Jet, ITCZ shifts, and atmospheric North–South linkages during abrupt climate changes of the last glacial period, Earth Planet. Sci. Let., 406, 233–246, doi:10.1016/j.epsl.2014.09.012, 2014.

Compo, G. P., Whitaker, J. S., Sardeshmukh, P. D., Matsui, N., Allan, R. J., Yin, X., Gleason, B. E., Vose, R. S., Rutledge, G., Bessemoulin, P., Brönnimann, S., Brunet, M., Crouthamel, R. I., Grant, A. N., Groisman, P. Y., Jones, P. D., Kruk, M. C., Kruger, A. C., Marshall, G. J., Maugeri, M., Mok, H. Y., Nordli, Ø., Ross, T. F., Trigo, R. M., Wang, X. L., Woodruff, S. D. and Worley, S. J.: The Twentieth Century Reanalysis Project, Q. J. Roy. Metor. Soc., 137, 1–28, doi:10.1002/qj.776, 2011.

Conley, D. and Schelske, C. L.: Biogenic silica, in Tracking environmental change using lake sediments; volume 3, terrestrial, algal, and siliceous indicators, vol. 3, Kluwer Academic Publishers, Dordrecht., 2001.

De Jonge, C., Hopmans, E. C., Zell, C. I., Kim, J.-H., Schouten, S. and Sinninghe Damsté, J. S.: Occurrence and abundance of 6-methyl branched glycerol dialkyl glycerol tetraethers in soils: Implications for palaeoclimate reconstruction, Geochim. Cosmochim. Ac., 141, 97–112, doi:10.1016/j.gca.2014.06.013, 2014.

Ebisuzaki, W.: A method to estimate the statistical significance of a correlation when the data are serially correlated, J. Climate, 10, 2147–2153, doi:10.1175/1520-0442(1997)010<2147:AMTETS>2.0.CO;2, 1997.

Formaterat: Teckensnitt:(Standard) Calibri

Formaterat: Normal

Formaterat: Engelska (USA)

Formaterat: Normal, Justera inte mellanrum mellan latinsk och asiatisk text, Justera inte mellanrum mellan asiatisk text och siffror

Formaterat: Engelska (USA)

Formaterat: Engelska (USA)

Formaterat: Engelska (USA)

Formaterat: Engelska (USA)

Formaterat: Engelska (USA)

Formaterat: Engelska (USA)

Formaterat: Engelska (USA)

Formaterat: Engelska (USA)

Formaterat: Engelska (USA)

Formaterat: Teckensnitt:(Standard) Calibri, Engelska (USA)

EPICA Community Members: One-to-one coupling of glacial climate variability in Greenland and Antarctica, Nature, 444, 195-198, doi:10.1038/nature05301 <http://doi.org/10.1038/nature05301> , hdl:10013/epic.41684, 2006.

Fogwill, C. J., Phipps, S. J., Turney, C. S. M. and Golledge, N. R.: Sensitivity of the Southern Ocean to enhanced regional Antarctic ice sheet meltwater input, Earth. Future, 3, 317–329, doi:10.1002/2015EF000306, 2015.

Gersonde, R., Crosta, X., Abelmann, A. and Armand, L.: Sea-surface temperature and sea ice distribution of the Southern Ocean at the EPILOG Last Glacial Maximum—a circum-Antarctic view based on siliceous microfossil records, Quaternary Sci. Rev., 24, 869–896, doi:10.1016/j.quascirev.2004.07.015, 2005.

Gottschalk, J., Skinner, L. C., Misra, S., Waelbroeck, C., Menviel, L. and Timmermann, A.: Abrupt changes in the southern extent of North Atlantic Deep Water during Dansgaard–Oeschger events, Nat. Geosci., 8, 950–954, doi:10.1038/ngeo2558, 2015.

Grasshoff, K., Erhardt, M. and Kremling, K.: Methods of sea water analysis, Verlag Chemie., 1983.

Hafsten, U.: Pleistocene development of vegetation and climate in Tristan de Cunha and Gough Island, Bergen, 1960.

Helfert, M., Mecking, O., Lang, F. and von Kaenel, H.-M.: Neue Perspektiven für die Keramikanalytik. Zur Evaluation der portablen energiedispersiven Röntgenfluoreszenzanalyse (P-ED-RFA) als neues Verfahren für die geochemische Analyse von Keramik in der Archäologie., Frankfurter elektronische Rundschau zur Altertumskunde, (14), 1–30, 2011.

Hogg, A. G., Hua, Q., Blackwell, P. G., Niu, M., Buck, C. E., Guilderson, T. P., Heaton, T. J., Palmer, J. G., Reimer, P. J., Reimer, R. W., Turney, C. S. M. and Zimmerman, S. R. H.: SHCal13 Southern Hemisphere Calibration, 0–50,000 Years cal BP, Radiocarbon, 55, 1889–1903, 2013.

Johnsen, S. J., Dahl-Jensen, D., Dansgaard, W. and Gundestrup, N.: Greenland palaeotemperatures derived from GRIP bore hole temperature and ice core isotope profiles, Tellus B: Chem. Phys. Meteor., 47, 624–629, doi:10.3402/tellusb.v47i5.16077, 1995.

Juggins, S.: User guide. Software for ecological and palaeoecological data analysis and visualisation, Newcastle University, Newcastle upon Tyne, UK., 2007.

Kaiser, J., Lamy, F. and Hebbeln, D.: A 70-kyr sea surface temperature record off southern Chile (Ocean Drilling Program Site 1233), Paleoceanography, 20, doi:10.1029/2005PA001146, 2005.

Krammer, K. and Lange-Bertalot, H.: Süsswasserflora von Mitteleuropa Bacillariophyceae Teil 1-4, Gustav Fisher, Stuttgart., 1986.

Lambeck, K., Rouby, H., Purcell, A., Sun, Y. and Sambridge, M.: Sea level and global ice volumes from the Last Glacial Maximum to the Holocene, PNAS, 111, 15296–15303, doi:10.1073/pnas.1411762111, 2014.

Lamy, F., Kilian, R., Arz, H. W., Francois, J.-P., Kaiser, J., Prange, M. and Steinke, T.: Holocene changes in the position and intensity of the southern westerly wind belt, Nat. Geosci., 3, doi:10.1038/ngeo959, 2010.

Lamy, F., Gersonde, R., Winckler, G., Esper, O., Jaeschke, A., Kuhn, G., Ullermann, J., Martinez-Garcia, A., Lambert, F. and Kilian, R.: Increased Dust Deposition in the Pacific Southern Ocean During Glacial Periods, Science, 343, 403–407, doi:10.1126/science.1245424, 2014.

Lange-Bertalot, H.: Diatomeen der Anden / Diatoms of the Andes., 1995.

Laskar, J., Robutel, P., Joutel, F., Gastineau, M., Correia, A. C. M. and Levrard, B.: A long-term numerical solution for the insolation quantities of the Earth, Ast. Astrophys., 428, 261–285, doi:10.1051/0004-6361:20041335, 2004.

Le Cohu, R. and Maillard, R.: Les diatomées monoraphidées des îles Kerguelen, Annal. Limnol., 19, 143–167, 1983.

Ljung, K. and Björck, S.: Holocene climate and vegetation dynamics on Nightingale Island, South Atlantic--an apparent interglacial bipolar seesaw in action, Quaternary Sci. Rev., 26, 3150–3166, doi:10.1016/j.quascirev.2007.08.003, 2007.

Ljung, K., Holmgren, S., Kylander, M., Sjolte, J., Van der Putten, N., Kageyama, M., Porter, C. T. and Björck, S.: The last termination in the central South Atlantic, Quaternary Sci. Rev., 123, 193–214, doi:10.1016/j.quascirev.2015.07.003, 2015.

Loomis, S. E., Russell, J. M., Ladd, B., Street-Perrott, F. A. and Sinninghe Damsté, J. S.: Calibration and application of the branched GDGT temperature proxy on East African lake sediments, Earth Planet. Sc. Lett., 357–358, 277–288, doi:10.1016/j.epsl.2012.09.031, 2012.

Markle, B. R., Bitz, C. M., Buizert, C., Steig, E. J., White, J. W. C., Pedro, J. B., Ding, Q., Schoenemann, S. W., Fudge, T. J., Sowers, T. and Jones, T. R.: Global atmospheric teleconnections during Dansgaard–Oeschger events, Nat. Geosci., 10, 36-40, doi:10.1038/ngeo2848, 2016.

Martin, J. H. and Fitzwater, S. E.: Iron deficiency limits phytoplankton growth in the north-east Pacific subarctic, Nature, 331, 341–343, doi:10.1038/331341a0, 1988.

Martínez-García, A., Sigman, D. M., Ren, H., Anderson, R. F., Straub, M., Hodell, D. A., Jaccard, S. L., Eglinton, T. I. and Haug, G. H.: Iron Fertilization of the Subantarctic Ocean During the Last Ice Age, Science, 343, 1347–1350, doi:10.1126/science.1246848, 2014.

McGee, D., Donohoe, A., Marshall, J. and Ferreira, D.: Changes in ITCZ location and cross-equatorial heat transport at the Last Glacial Maximum, Heinrich Stadial 1, and the mid-Holocene, Earth Planet. Sci. Lett., 390, 69–79, doi:10.1016/j.epsl.2013.12.043, 2014.

Millo, C., Strikis, N. M., Vonhof, H. B., Deininger, M., Cruz, F. W. da, Wang, X., Cheng, H. and Edwards, R. L.: Last glacial and Holocene stable isotope record of fossil dripwater from subtropical Brazil based on analysis of fluid inclusions in stalagmites, Chem. Geol., 468, 84–96, doi:10.1016/j.chemgeo.2017.08.018, 2017.

Moore, P. D., Webb, J. A. and Collinson, M. E.: Pollen analysis, 2ed ed., Blackwell Scientific, Oxford., 1991.

Moser, G., Steindorf, A. and Lange-Bertalot, H.: Neukaledonien Diatomeenflora einer Tropeninsel. Revision der Collection Maillard und Untersuchung neuen Materials., Bibliotheca Diatomologia, 32, 1–340, 1995.

Naafs, B. D. A., Inglis, G. N., Zheng, Y., Amesbury, M. J., Biester, H., Bindler, R., Blewett, J., Burrows, M. A., Torres, D. del C., Chambers, F. M., Cohen, A. D., Evershed, R. P., Feakins, S. J., Gałka, M., Gallego-Sala, A., Gandois, L., Gray, D. M., Hatcher, P. G., Coronado, E. N. H., Hughes, P. D. M., Huguet, A., Könönen, M., Laggoun-Défarge, F., Lähteenoja, O., Lamentowicz, M., Marchant, R., McClymont, E., Pontevedra-Pombal, X., Ponton, C., Pourmand, A., Rizzuti, A. M., Rochefort, L., Schellekens, J., Vleeschouwer, F. D. and Pancost, R. D.: Introducing global peat-specific temperature and pH calibrations based on brGDGT bacterial lipids, Goechim. Cosmochim. Ac., 208, 285–301, doi:10.1016/j.gca.2017.01.038, 2017.

938 Nesbitt, H. W. and Young, G. M.: Early Proterozoic climate and plate motions inferred from major
939 element chemistry of lutites, Nature, 299, 715–717, 1982.

940 Pearson, E. J., Juggins, S., Talbot, H. M., Weckström, J., Rosén, P., Ryves, D. B., Roberts, S. J. and
941 Schmidt, R.: A lacustrine GDGT-temperature calibration from the Scandinavian Arctic to Antarctic:
942 Renewed potential for the application of GDGT-paleothermometry in lakes, Geochim. Cosmochim.
943 Ac., 75, 6225–6238, doi:10.1016/j.gca.2011.07.042, 2011.

944 Pedro, J. B., Martin, T., Steig, E. J., Jochum, M., Park, W. and Rasmussen, S. O.: Southern Ocean deep
945 convection as a driver of Antarctic warming events, Geophys. Res. Lett., 43, 2016GL067861,
946 doi:10.1002/2016GL067861, 2016.

947 Pedro, J. B., Jochum, M., Buizert, C., He, F., Barker, S. and Rasmussen, S. O.: Beyond the bipolar
948 seesaw: Toward a process understanding of interhemispheric coupling, Quaternary Sci. Rev., 192, 27–
949 46, doi:10.1016/j.quascirev.2018.05.005, 2018.

950 Ryan, P.: Field guide to the animals and plants of Tristan da Cunha and Gough Island, Pisces
951 publications, Newbury., 2007.

952 Saunders, K. M., Roberts, S. J., Perren, B., Butz, C., Sime, L., Davies, S., Van Nieuwenhuyze, W.,
953 Grosjean, M. and Hodgson, D. A.: Holocene dynamics of the Southern Hemisphere westerly winds
954 and possible links to CO2 outgassing, Nat. Geosci., 11(9), 650–655, doi:10.1038/s41561-018-0186-5,
955 2018.

956 Sime, L. C., Kohfeld, K. E., Le Quéré, C., Wolff, E. W., de Boer, A. M., Graham, R. M. and Bopp, L.:
957 Southern Hemisphere westerly wind changes during the Last Glacial Maximum: model-data
958 comparison, Quaternary Sci. Rev., 64, 104–120, doi:10.1016/j.quascirev.2012.12.008, 2013.

959 Sime, L. C., Hodgson, D., Bracegirdle, T. J., Allen, C., Perren, B., Roberts, S. and de Boer, A. M.: Sea
960 ice led to poleward-shifted winds at the Last Glacial Maximum: the influence of state dependency on
961 CMIP5 and PMIP3 models, Clim. Past, 12, 2241–2253, doi:10.5194/cp-12-2241-2016, 2016.

962 Sjolte, J., Sturm, C., Adolphi, F., Vinther, B. M., Werner, M., Lohmann, G. and Muscheler, R.: Solar
963 and volcanic forcing of North Atlantic climate inferred from a process-based reconstruction, Clim.
964 Past ,14, 1179-1194, https://doi.org/10.5194/cp-14-1179-2018, 2018.

965 Stenni, B., Masson-Delmotte, V., Selmo, E., Oerter, H., Meyer, H., Röthlisberger, R., Jouzel, J.,
966 Cattani, O., Falourd, S., Fischer, H., Hoffman, G., Iacumin, P., Johnsen, S. J., Minster, B. and Udisti,
967 R.: The deuterium excess records of EPICA Dome C and Dronning Maud Land ice cores (East
968 Antarctica), Quaternary Science Reviews, 29, 146–159, doi:Stenni, B.; Masson-Delmotte, V.; Selmo,
969 E.; Oerter, H.; Meyer, H.; Röthlisberger, R; Jouzel, J.; Cattani, O.; Falourd, S.; Fischer, H.; Hoffman,
970 G.; Iacumin, P.; Johnsen, S.J.; Minster, B.; Udisti, R.. 2010 The deuterium excess records of EPICA
971 Dome C and Dronning Maud Land ice cores (East Antarctica). Quaternary Sci. Rev., 29 . 146-159.
972 https://doi.org/10.1016/j.quascirev.2009.10.009 <https://doi.org/10.1016/j.quascirev.2009.10.009>,
973 2010.

974 Stocker, T. F. and Johnsen, S. J.: A minimum thermodynamic model for the bipolar seesaw,
975 Paleoceanography, 18, PA000920, doi:200310.1029/2003PA000920, 2003.

976 Tierney, J. E. and deMenocal, P. B.: Abrupt Shifts in Horn of Africa Hydroclimate Since the Last
977 Glacial Maximum, Science, 342, 843–846, doi:10.1126/science.1240411, 2013.

978 Toggweiler, J. R. and Lea, D. W.: Temperature differences between the hemispheres and ice age
979 climate variability, Paleoceanography, 25, PA2212, doi:10.1029/2009PA001758, 2010.

Toggweiler, J. R., Russell, J. L. and Carson, S. R.: Midlatitude westerlies, atmospheric CO2, and climate change during the ice ages, Paleoceanography, 21, PA2005, doi:200610.1029/2005PA001154, 2006.

Van de Vijver, B., Beyens, L. and Lange-Bertalot, H.: Freshwater diatoms from Ile de la Possession (Crozet Archipelago, Subantarctic), J. Cramer, Berlin., 2002.

Veres, D., Bazin, L., Landais, A., Toyé Mahamadou Kele, H., Lemieux-Dudon, B., Parrenin, F., Martinerie, P., Blayo, E., Blunier, T., Capron, E., Chappellaz, J., Rasmussen, S. O., Severi, M., Svensson, A., Vinther, B. and Wolff, E. W.: The Antarctic ice core chronology (AICC2012): an optimized multi-parameter and multi-site dating approach for the last 120 thousand years, Clim. Past, 9, 1733–1748, doi:10.5194/cp-9-1733-2013, 2013.

Waelbroeck, C., Labeyrie, L., Michel, E., Duplessy, J. C., McManus, J. F., Lambeck, K., Balbon, E. and Labracherie, M.: Sea-level and deep water temperature changes derived from benthic foraminifera isotopic records, Quaternary Sci. Rev., 21, 295–305, doi:10.1016/S0277-3791(01)00101-9, 2002.

WAIS Divide Project Members: Precise interpolar phasing of abrupt climate change during the last ice age, Nature, 520, 661–665, doi:10.1038/nature14401, 2015.

Weber, M. E., Clark, P. U., Kuhn, G., Timmermann, A., Sprenk, D., Gladstone, R., Zhang, X., Lohmann, G., Menviel, L., Chikamoto, M. O., Friedrich, T. and Ohlwein, C.: Millennial-scale variability in Antarctic ice-sheet discharge during the last deglaciation, Nature, 510, 134, doi:10.1038/nature13397, 2014.

Weijers, J. W. H., Schefuss, E., Schouten, S. and Damste, J. S. S.: Coupled Thermal and Hydrological Evolution of Tropical Africa over the Last Deglaciation, Science, 315, 1701–1704, doi:10.1126/science.1138131, 2007.

Werner, M., Haese, B., Xu, X., Zhang, X., Butzin, M. and Lohmann, G.: Glacial–interglacial changes in H218O, HDO and deuterium excess – results from the fully coupled ECHAM5/MPI-OM Earth system model, Geosci. Model Dev., 9, 647–670, doi:10.5194/gmd-9-647-2016, 2016.

Yamoah, K. A., Chabangborn, A., Chawchai, S., Schenk, F., Wohlfarth, B. and Smittenberg, R. H.: A 2000-year leaf wax-based hydrogen isotope record from Southeast Asia suggests low frequency ENSO-like teleconnections on a centennial timescale, Quaternary Sci. Rev., 148, 44–53, 2016.

Zhu, C., Lipp, J. S., Wörmer, L., Becker, K. B., Schröder, J. M. and Hinrichs, K.-U.: Comprehensive glycerol ether lipid fingerprints through a novel reversed phase liquid chromatography–mass spectrometry protocol, Org. Geochem., 65, 53–62, doi:10.1016/j.orggeochem.2013.09.012, 2013.